Using Micro-Doppler Radar Signals for Human Gait Detection

by

Adel Alzogaiby

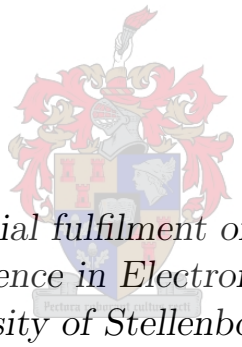

Thesis presented in partial fulfilment of the requirements for the degree Master of Science in Electronic Engineering at the University of Stellenbosch.

Department of Electrical and Electronic Engineering,
University of Stellenbosch,
Private Bag X1, Matieland 7602, South Africa.

Supervisor: Prof. G-J van Rooyen

December 2013

Declaration

By submitting this thesis electronically, I declare that the entirety of the work contained therein is my own, original work, that I am the sole author thereof (save to the extent explicitly otherwise stated), that reproduction and pub- lication thereof by Stellenbosch University will not infringe any third party rights and that I have not previously in its entirety or in part submitted it for obtaining any qualification.

Signature Date

Abstract

This work entails the development and performance analysis of a human gait detection system based on radar micro-Doppler signals. The system consists of a tracking functionality and a target classifier. Target micro-Doppler signatures are extracted with Short-Time Fourier Transform (STFT) based spectrogram providing a high-resolution signatures with the radar that is used. A feature extraction mechanism is developed to extract six features from the signature and an artificial neural network (A-NN) based classifier is designed to carry out the classification process. The system is tested on real X-band radar data of human subjects performing six activities. Those activities are walking and speed walking, walking with hands in pockets, marching, running, walking with a weapon, and walking with arms swaying. The multiclass classifier was designed to discriminate between those activities. High classification accuracy of 96% is demonstrated.

Abstract

Hierdie werk behels die ontwikkeling, en analise van werksverrigting, van 'n menslike stapdetekor gebaseer op radar-mikrodoppleranalise. Die stelsel bestaan uit 'n teikenvolger en -klassifiseerder. Die mikrodoppler-kenmerke van 'n teiken word met behulp van die korttyd-Fourier-transform onttrek, en verskaf hoë-resolusie-kenmerke met die radar wat vir die implementering gebruik word. 'n Kenmerkontrekkingstelsel is ontwikkel om ses kenmerke vanuit die spektrogram te onttrek, en 'n kunsmatige neurale netwerk word as klassifiseerder gebruik. Die stelsel is met 'n X-band radar op werklike menslike beweging getoets, terwyl vrywilligers ses aktiwiteite uitgevoer het: loop, loop (hand in die sakke), marsjeer, hardloop, loop met 'n wapen, loop met arms wat swaai. Die multiklas-klassifiseerder is ontwerp om tussen hierdie aktiwiteite te onderskei. 'n Hoë klassifiseringsakkuraatheid van 96% word gedemonstreer.

Acknowledgements

I'd like to express my thanks and gratitude;
To my parents, family, and friends, for their love and prayers;
To my employer for the great opportunity to do this work;
To my friends and colleagues at KACST, RRS, and Stellenbosch university for generously allowing me to use their resources;
And most thanks to my supervisor, Gert-Jan van Rooyen, for ultimate support and creative discussions throughout my study.

Contents

List of Figures

List of Tables

Nomenclature

Acronyms	Description
ADC	Analogue to Digital Converter
BD	B-Distribution
CA-CFAR	Cell-Averaging Constant False Alarm Rate
CFAR	Constant False Alarm Rate
CNR	Clutter to Noise Ratio
CPI	Coherent Processing Interval
CW	Continuous Wave
DC	Direct Current (0 Hz frequency)
DCT	Discrete Cosine Transform
DFFT	Doppler FFT
DTFT	Discrete-Time Fourier Transform
DTW	Dynamic Time Wrapping
ECM	Electronic Counter Measures
EMI	Electromagnetic Interference
FFT	Fast Fourier Transform
FMCW	Frequency-Modulated Continuous-Wave
GD	Gait-Doppler
GMM	Gaussian Mixture Model
I	In-phase component
LADAR	Laser Detection and Ranging
LDA	Linear Discriminant Analysis
LOS	Line of sight
MTI	Moving Target Indicator
PCA	Principal Component Analysis
PF	Particle Filter
PPI	Plan Position Indicator
PRF	Pulse Repetition Rrequency
PRI	Pulse Repetition Interval
PWVD	Pseudo Wigner-Ville Distribution
Q	Quadrature component

RCS	Radar Cross Section
RD	Range-Doppler
RFFT	Range FFT
RHS/LHS	Right-Hand Side/Left-Hand Side
RRS	Ruetech Radar Systems.
RSR940	Reutech Spider Surveillance Radar System
STFT	Short-Time Fourier Transform
SVM	Support Vector Machine
WVD	Wigner-Ville Distribution

Variables	Description
A	Amplitude of transmitted radar signal
A'	Amplitude of received radar signal
A_{f_D}	Amplitude at the average Doppler frequency f_D
A_{f_m}	Amplitude at the fundamental frequency f_m
A_{f_3}	Amplitude at the 2^{nd} harmonic frequency f_3
A_{f_3}	Amplitude at the 3^{rd} harmonic frequency f_3
β_1, β_2	Frequency ratios
$B_{\mu D}$	Doppler bandwidth with micro-Doppler
B_W	Doppler bandwidth
c	Speed of light
$\delta\phi$	Phase difference
f_0	Transmitted frequency
f_2, f_3	Harmonic frequencies
f_{av}	Average Doppler frequency
f_D	Doppler frequency shift
f_m	Fundamental gait frequency (also Stride Rate)
f_r	Received signal frequency
f_v	Vibration frequency
k	Frequency index
K	Number of Doppler bins
k	Doppler bins index number
k	Discrete frequency index
L	Number of range bins
l	Range bin count number
λ_0	Wavelength of transmitted signal
L_s	Stride length
M	Number of Pulses or sweeps
m	Pulse count number
n	Discrete time index
N	Number of discrete time samples
N_{FFT}	Number of points in DTFT
P_{FA}	Probability of False Alarm
ϕ	micro-Doppler phase offset
ψ	Target angle with respect to the radar LOS
R_0	Range of the target
s_D	Doppler complex signal
$s_r(t)$	Received signal
$s_t(t)$	Transmitted signal
t	Time

T	Period
τ	Pulse width
θ	Signal phase
θ'	Phase shift
t_m	Transmit time for the m^{th} pulse
v_{av}	Average radial velocity
v_r	Radial velocity
w	FFT weighting window

Chapter 1

Introduction

1.1 The Need for Human Detection

The use of radar to protect land and borders against intruding surface targets, such as humans and vehicles, has shown a great advantage over optical, infrared, and acoustical systems. Radars transmit and receive RF energy that interacts with targets and the surrounding environment, in order to detect targets and separate them from the environment.

However, it is often a requirement that targets be classified, rather than only detected. Although a skilled operator can identify targets by listening to the downmixed Doppler audio signal, this solution is not always practical – especially if the radar is deployed in a remote location. In this thesis, we provide a solution that automates this classification process.

In general, moving targets introduce the Doppler effect in the returned radar signal that is directly related to the moving dynamics of the target. With recent technology and advancement in signal processing, it is possible to extend the capabilities of the radar to automatically recognise the targets from the characteristics of the returned signal influenced by the target dynamics.

Recent studies, which we will present next, show that targets with moving parts introduce additional Doppler components, called micro-Doppler signals, that modulate the main Doppler contribution of the target. Moreover, it shows a unique signature which then can be observed and analysed to extract key information that allows recognition with high accuracy.

In this work, a study of the subject of micro-Doppler effect in radar is presented, along with the design and implementation of a human-gait classification system. This work will add a new functionality to an existing surveillance radar system to be able to automatically classify human targets.

The classification process presented in this work combines two methods from the literature and made suitable for practical implementation. Radar data of humans performing different activities was recorded for the purpose of this work.

1.2 Literature Review

In radar, the subject of human-gait classification falls under the field of radar target recognition. The topic of target recognition is as significant and early as the radar itself. There is always a demand, not only to detect, but to also determine the type of the radar target. The development and advancement in this field focus on automating the recognition process and analysing the scattered signal to extract more useful information. The classical radar target recognition techniques are thoroughly discussed in [15], [16], [17], [18], and [19]. Most of those techniques focus on studying the scattering effects gained by the geometrical aspects of the target, such as the range-profile and polarisation effects. The target's Doppler shift is also used to aid in the recognition process but only as an overall velocity of the target [16]. Those parameters are used to estimate the shape of the target which is then used for recognition. With some types of targets, such as humans, it becomes very difficult to rely on the geometrical aspects of the target due to its ultimate complexity which demands an ultra-high resolution range.

In radar, what is now known as the micro-Doppler effect was first discovered in the audio of the Doppler signal which can be heard through speakers. Different targets create unique audio signatures that a well-trained operator can hear in the Doppler audio signal, and some operators can even recognise the type of target [16]. As we'll show in the following paragraphs, this Doppler effect has recently been investigated in different domains to automate the recognition process. A good introduction to the micro-Doppler phenomenon is found in [1] and [28].

Before we discuss the literature in micro-Doppler signature-based target classification, it is useful to list the key aspects considered in literature, namely

- the techniques used to extract and visualise the micro-Doppler signals from the raw radar data;
- prediction and verification of micro-Doppler signals via modelling and simulation;
- recording and visualisation of signatures from real data of various types

of targets, and the type of radar platform employed or designed for that purpose;

- representation of those signatures with unique feature-sets; and
- the classification techniques used.

Micro-Doppler Representation Techniques

The representation of micro-Doppler signatures is often carried out in the time-frequency domain. In most cases, the Short Time Frequency Transform (STFT)-based spectrogram is used to extract the signature [64, 37, 43, 33]. Depending on the data being used, the dynamics of the target can be observed in the signature, and this usually provides sufficient input for classification. Other time-frequency representations are also used which can either present more information from the raw radar data [20], or provide higher resolution spectral images [60, 1]. A good overview of time-frequency analysis is found in [7]. For radar applications, various time-frequency analysis techniques, including Doppler-based imaging, are discussed in [27]. Some common time-frequency analysis techniques are evaluated and applied to micro-Doppler phenomenon in [1] and [28]. The author of [43] uses the chirplet transform to represent the micro-Doppler signature. Although it represents a better model for the signature, it is difficult to relate the model to the dynamics of the target. The author of [60] evaluates additional time-frequency distributions besides the spectrogram, as applied to human-induced micro-Doppler signals. These are the Pseudo-Wigner-Ville Distribution (PWVD) and the B-Distribution (BD). The B-Distribution has also been investigated in [56] for basic micro-Doppler signatures such as rotation and vibration. The S-method, which is derived from the WVD, is used to represent the target signature in [66]. The Reassigned-Transform and the Iterative Adaptive Approach are two advanced techniques that have been investigated in [49], [52], [44], [48], and [65]. These were proposed to sharpen the micro-Doppler signature of the target. This leads to a better resolution that allows decomposition of the micro-Doppler components. An attempt to decompose the micro-Doppler signature was made in [67] by using the Hough Transform. The Wavelet Transform has been used in [70] to extract the micro-Doppler signature.

Micro-Doppler Signatures from Simulated and Real Data

There are few micro-Doppler target models found in literature. The models are then used to visualise the micro-Doppler effect of common targets [1],

as well as to verify recorded-data [28]. [28] simulates the micro-Doppler signature of four types of motion: rotation, vibration, coning, and tumbling[1]. This work has been extended in [1] to simulate real targets such as humans, animals, birds, and helicopters. In [68], Garbuz simulates micro-Doppler signatures from a 12-point model of a walking human. High resolution data from a human pedestrian model provided by a motion capture system was simulated in [32]. This model includes humans walking and running at different elevation and azimuth aspect angles, demonstrating their effect on the micro-Doppler signal. Another simulation was carried out in [31] with a 15-point motion model. The authors of [41] use a human locomotion model to generate data that was used to provide a priori-knowledge to the target classification process.

Micro-Doppler effect can also be observed in recorded data. A remarkable effort was done by [22] and [57] who collected and investigated different target signatures of humans performing different activities; vehicles, animals, and clutter. Further significant work was done by [33] and [34], who investigated their techniques on four human subjects, which each performed seven different activities. [30], [31], [63], and [69] present micro-Doppler signatures of humans walking and cycling, vehicle, and animals. Data from wheeled and tracked vehicles were found in [71], [20], [61], and [62]. Data from single, pairs, and groups of people were collected and examined in [36].

Feature Extraction

Feature extraction is a process that is normally required prior to target classification. Different techniques for micro-Doppler feature extraction are found in literature. Some techniques are only designed for one type of target (e.g. human) and others are designed for different types of targets. A simple method to extract features from human micro-Doppler signatures is presented in [64]. This method is carried out by cross-correlating one spectrogram time-frame with the previous one, in which, once the human target is present, the correlation will generate detectable peaks. Another simple method is found in [71] which allows for target classification based only on the target velocity. Stride rate, which is the rate at which a human makes one step, is presented in [30] and [31]. On its own, this feature is found to be descriptive, but not suitable enough for human target classification. [37], [38], and [53] define two features for human signatures: velocity and step frequency. The later is defined as the difference in Doppler frequency between the legs' Doppler-envelope and the body's Doppler contribution. It is shown that the first is

[1]Tumbling is a rotation accompanied by translation and acceleration. Coning is a rotation of a rigid body around a cone's circle [28].

always a constant multiple of the second for the periodic human motion. The authors of [24] and [35] use the dominant geometrical lines extracted from the signature to represent the micro-Doppler features of rotation, vibration, coning, and tumbling. The authors of [33] and [34] use image-based techniques such as edge detection to represent the signatures from seven different human activities with a feature set of eight values. In [23], the author uses three features that distinguish human motion from other types of motion: average velocity, stride-rate, and an Radar-Cross-Section (RCS)-based ratio.

The techniques mentioned so far can be directly related to the target dynamics. Other techniques are employed for micro-Doppler feature extraction that are generally known in signal and speech processing but difficult to relate to the target dynamics. [20], [61], and [62] introduce Dynamic Time Wrapping (DTW), a technique more often used in speech recognition technique, to extract features from different target signatures. The cepstrum, which is also a technique that is often used in speech processing, is used in [39] to represent the target signature with a set of cepstral coefficients. Statistical-based methods such as the Gaussian-Mixture-Model (GMM) and Particle Filter (PF) are introduced in [41] and [54], respectively, for feature extraction. The Discrete Cosine Transform (DCT) is implemented in [36] for feature extraction. Some techniques may produce large feature-sets. In this case, Principal Component Analysis (PCA) can be used to reduce the size of the feature set. This technique is used in [20] and [25].

Classification Techniques

Many experiments and performance evaluations of various micro-Doppler classification techniques are found in literature. A simple classification method such as Linear Discriminant Analysis (LDA) may be employed, as done in [71] and [23]. Support Vector Machine (SVM) and Artificial Neural Network (A-NN) based classifiers have shown good classification performance [37, 38, 53, 24, 35, 33, 34]. Other classification methods include k-nearest neighbour (k-nn), and naïve Bayesian classifiers [20], [62], and [24]. A comparison between various classifiers can be found in [35], [25], and [24]. Most of the presented studies show that, if the target's feature set is well defined, it is easily recognised, regardless of the classification technique used.

Testing and Development Platform

Most of the aforementioned studies either developed a radar system for testing of algorithms and capturing data, or used an existing system. A Continuous-Wave (CW) radar operating at 24 GHz was developed in [64]

and [38] to detect humans in real time. The classifier in [71] was developed and tested for an existing Ku-band radar (MSTAR) to operate in scanning mode, replacing the Doppler-audio-based operator. A complete X-band CW radar system was developed in [43] for micro-Doppler human-gait analysis. [21] describes the design and testing of a multi-target tracking radar system with human classification. A multi-channel X-band radar system was developed in [22] and [57] to demonstrate micro-Doppler signatures of a wide variety of targets. It is useful to point out that, as found in most of the literature, a higher radar frequency results in a better Doppler resolution.

1.3 Thesis Objectives

The goals to be achieved in this project are summarised as follows:

- The subject of micro-Doppler phenomenon will be studied in order to better identify how micro-Doppler features relate to a target and its movements.
- A practical and reliable method to extract micro-Doppler information from the radar data will be developed.
- Radar parameters that have an effect in the resolution of micro-Doppler information will be identified.
- A full micro-Doppler feature extractor will be developed that combines two methods from literature with some enhancements.
- Simple and a multi-class classifiers will be implemented that can classify human targets based on the extracted features.
- The system will be trained using real radar data, and tested using separate data set.

1.4 Contribution

Contributions made in this work are:

1. A human target classification system that works in real-time in conjunction with an existing radar system.
2. Implementation of a feature extraction mechanism that combines two methods.

3. Implementation of a multi-class classifier that has the potential to recognise other types targets such as animals and vehicles.

1.5 Thesis structure

A theoretical background of all the topics discussed in this work is given in chapter 2. Chapter 3 discusses the conceptual design of the human gait detection system. Detailed design of the system is given in chapter 4. Testing and evaluation of the system with real radar data are presented in chapter 5. Finally, our concluding remarks and suggestions for further work are given in chapter 6.

Chapter 2

Theoretical Background

2.1 Introduction

The Doppler effect has been studied in numerous fields and applications of science and engineering [18]. In radar, the effect can be seen as a shift in the frequency of the reflected signals from moving targets [3].

Radar transmits electromagnetic waves to detect objects of interest by receiving the returned echoes from those objects [18]. The radar can locate those objects based on the time delay between transmitting and receiving the signal. If one object is moving, a frequency shift will be induced in the returned signal, which is caused by the Doppler effect.

The Doppler effect varies depending on the radial velocity of the object with respect to the radar. Besides measuring the radial velocity of a target, modern radars use the Doppler effect to eliminate moving targets from stationary clutter, which enhances the process of target detection [18].

If the object has oscillating, rotating, or vibrating parts, those parts will induce additional Doppler components that modulate about the main Doppler component which was caused by the bulk motion. Those additional components are called the *micro-Doppler* components [1, 28].

Extraction of micro-Doppler information can lead to a better representation of the target dynamics. With additional processing, recognition of the target is possible [24]. In the case of human targets, the micro-Doppler components correspond to the swinging of arms and legs while walking or running; they modulate about the main Doppler component induced by the bulk motion of the torso.

In the following sections we give background information on how the Doppler shift is commonly estimated in a radar signal. The most commonly used method to extract Doppler information is presented. The micro-Doppler

effect will then be introduced, along with a method for extracting the target signature by means of joint time-frequency analysis. Some examples of micro-Doppler signatures of selected targets will be shown. Further analysis of micro-Doppler signatures that leads to target recognition which involve feature extraction and pattern recognition techniques are presented.

2.2 Doppler Effect in Radar

Due to the Doppler effect, the frequency of the received signal f_r from a moving point scatterer will differ from the transmitted frequency f_0. The special relativity theorem predicts that the received frequency f_r can be represented as [1, 3]

$$f_r = \left(\frac{1 + v_r/c}{1 - v_r/c}\right) f_0 \tag{2.1}$$

where v_r is the radial velocity of the scatterer with respect to the source. Since the velocity of actual radar targets is very small compared to the speed of light ($v_r \ll c$), Equation 2.1 can be reduced to [3]

$$f_r = \left[1 + 2\frac{v_r}{c}\right] f_0 \tag{2.2}$$

The difference between the transmitted frequency f_0 and the received frequency f_r is the Doppler shift, f_D

$$f_r - f_0 = f_D = \frac{2v_r}{c} f_0 = \frac{2v_r}{\lambda_0} \tag{2.3}$$

where λ_0 is the transmitted wavelength and v_r is positive for an approaching target and negative for a receding target.

If the target is moving with velocity v and an angle ψ with respect to the radar line-of-sight, where $\psi = 0$ for an approaching target and 180° for a receding target, the radial velocity will become $v \cdot \cos\psi$ and Equation 2.3 becomes

$$f_D = \frac{2v}{\lambda_0} \cos\psi \tag{2.4}$$

Therefore, the Doppler shift is at a maximum if the target is travelling directly inbound or outbound ($\psi = 0$ or 180°). If the target is crossing the beam of the radar tangentially ($\psi = 90°$) then f_D will equal 0 Hz.

The above equation only shows the physical relationship between the Doppler shift and the radial velocity of the target. It cannot be used to extract the Doppler information, since the radial velocity of the target is unknown and more than one target may be present. The following section shows how to extract Doppler information in modern radars.

2.3 Extraction of Doppler Information

For a pulse radar, each pulse, whether it is modulated or not, exhibits a certain limited significant bandwidth. Targets that are not fast enough would only cause a small Doppler shift that is not large enough to exceed the bandwidth of one pulse. For this reason, it is very difficult to estimate Doppler shift based on a single pulse [3]. Therefore, the use of multiple pulses to measure the Doppler shift is essential, as will be shown in the following sections.

2.3.1 Video Detectors and Coherent Detectors

Let us assume a single sinusoidal pulse transmitted with a carrier frequency f_0 and centred at time $t = 0$:

$$s_0(t) = A\cos(2\pi f_0 t + \theta), \quad -\frac{\tau}{2} \leq t \leq \frac{\tau}{2} \tag{2.5a}$$

If the carrier frequency f_0 is known, the pulse can be characterised with its amplitude A and phase θ within its period τ:

$$s_0(t) = \mathbf{Re}\left\{Ae^{j(2\pi f_0 t+\theta)}\right\} \tag{2.5b}$$

$$= \mathbf{Re}\left\{(Ae^{j\theta})e^{j2\pi f_0 t}\right\} \tag{2.5c}$$

If the transmitted pulse in Equation 2.5 reflects from a target at range R_0, the radar will receive the pulse at time $t' = 2R_0/c$. The received pulse will be

$$s_r(t) = s_0\left(t - \frac{2R_0}{c}\right) \tag{2.6a}$$

$$= A'\cos\left[\pi f_0\left(-\frac{2R_0}{c} + \theta\right)\right] \tag{2.6b}$$

$$= A'\cos\left(2\pi f_0 t + \theta - \frac{4\pi}{\lambda}R_0\right) \tag{2.6c}$$

$$= A'\cos(2\pi f_0 t + \theta'), \quad -\frac{\tau}{2} + \frac{2R_0}{c} \leq t \leq \frac{\tau}{2} + \frac{2R_0}{c} \tag{2.6d}$$

$$= \mathbf{Re}\left\{(A'e^{j\theta'})e^{j2\pi f_0 t}\right\} \tag{2.6e}$$

The received pulse has a new amplitude $A^{'}$ which is attenuated according to the radar range equation, a new phase $\theta' = \theta - \frac{4\pi}{\lambda}R_0$, and is delayed in time by $2R_0/c$. The phase of the received pulse (θ) is shifted by $-4\pi R_0/\lambda$ and is proportional to the range of the target. If the target travels with a constant

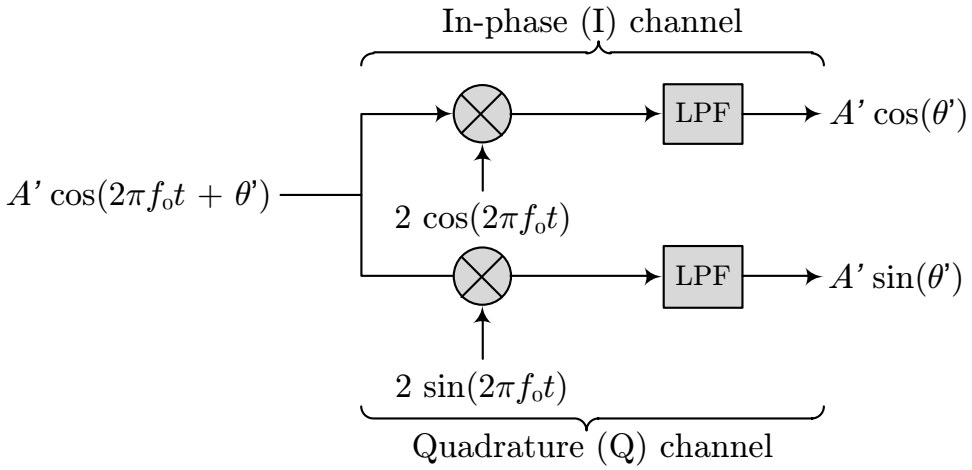

Figure 2.1: Classical coherent I/Q detector.
$\theta' = \theta - \frac{4\pi}{\lambda_0} R_0$ (reproduced from [3]).

velocity, the rate of change of its phase will be constant. If the targets accelerate or decelerate, the rate of change of phase will vary accordingly. These two facts are the key to Doppler and micro-Doppler estimation in modern radars.

The unknown parameters of the received pulse in equation 2.6 are the new amplitude A', the phase shift θ', and the time delay $t_0 = 2R_0/c$. Radars are designed to measure those parameters. Modern radars employ the coherent detector to extract the in-phase and quadrature components of the input received signal. In addition, the moving direction of the target can be found. A general form of the coherent detector is shown in figure 2.1. This configuration splits the incoming signal into two channels. The upper channel signal is mixed with the reference oscillator, while the other channel is mixed with a 90° shifted reference signal. By working out the output of the two mixers and the low-pass filters, the output of the two channels are found to be

$$I = A' \cos\theta' \tag{2.7a}$$
$$Q = A' \sin\theta' \tag{2.7b}$$

Combining the I and Q components gives the complex baseband form of the received signal

$$s_r = I + jQ \tag{2.8a}$$
$$= A'(\cos\theta' + j\sin\theta') \tag{2.8b}$$
$$= A' e^{j\theta'} \tag{2.8c}$$

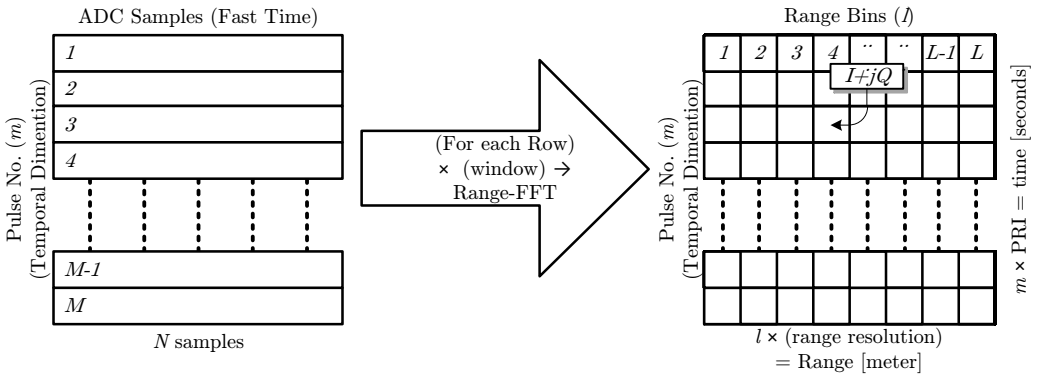

Figure 2.2: Resolving range from ADC samples: The data matrix is shown on the right-hand side. Each row forms one range swath.

As we can see, the complex output allows independent measurement of amplitude and phase as well as the direction of the target by means of positive or negative Doppler shifts.

2.3.2 Range Bins and Data Matrix

The use of a coherent detector allows measurement of the received signal's amplitude and phase. The time delay of the received echo is estimated by sampling the output of the receiver repeatedly after the pulse is transmitted and observing the time at which the echo was received.

For each time sample, whenever a received pulse is present, the output of the receiver is sampled and a complex signal with I and Q components is formed. The vector of samples that is formed from the output of the receiver for each pulse is called the *fast-time* vector. A form of pulse-compression processing is performed on this vector to resolve the range information. The output of this process is a vector of the same length called the *range swath* and each of its elements is called a *range bin* (Figure 2.2).

When the radar transmits M pulses in a dwell time (which is the time an antenna beam spends on a target), a set of range bins will be generated for each pulse. Those are typically stored in memory as a two dimensional matrix of complex samples as shown in Figure 2.2. The time interval between samples in a row equals one Pulse Repetition Interval (PRI), so the sample rate in this dimension is the Pulse Repetition Frequency (PRF). Each row of the matrix represents a series of measurements from the same range bin over M successive pulses. The total amount of time MT represented by the data matrix is the Coherent Processing Interval (CPI) [3].

2.4 Doppler Signal

Suppose a target is approaching the radar with radial velocity v and the radar transmits a series of M pulses separated by a PRI of T seconds. The range to the target when the m^{th} pulse is transmitted is $R_0 - mvT$ meters. The phase shift of the echo of the m^{th} pulse will be

$$\Delta\theta = (-4\pi/\lambda)(R_0 - vmT) \quad [\text{rad}]$$

When the output of the coherent detector is sampled some time during the echo, the measured output for the m^{th} pulse will be

$$s_D[m] = A\exp\left\{j[\theta - (4\pi/\lambda)(R_0 - vmT)]\right\} \tag{2.9a}$$

$$= A\exp\left\{j\left[2\pi\frac{2v}{\lambda}(mT) + \theta - \left(\frac{4\pi R_0}{\lambda}\right)\right]\right\} \tag{2.9b}$$

substituting for f_D in Equation 3.1 yields:

$$s_D[m] = A\exp\left[j(2\pi f_D t_m + \theta')\right], \quad \leq m \leq M-1 \tag{2.9c}$$

where $t_m = mT$ is the transmit time for the m^{th} pulse. Equation 2.9 shows that the sampled signal formed by measuring the phase of each successive pulse echo with a multi-pulse waveform forms a discrete-time complex sinusoid at the expected Doppler frequency.

The signal is sampled at instants t_m separated by the PRI. The sinusoid is the result of the changing echo phases which are caused by the changes in target range between pulses. Doppler shift measured from a series of phase measurements in this way is referred to as *spatial Doppler* [3].

2.4.1 The Doppler Spectrum

The output signal of the coherent detector is the superposition of some or all of the following components:

- echoes from moving or non-moving targets,
- clutter,
- receiver and atmospheric noise,
- spurious signals from the receiver, and
- intended interference signals (electronic countermeasures) or non-intended interference signals.

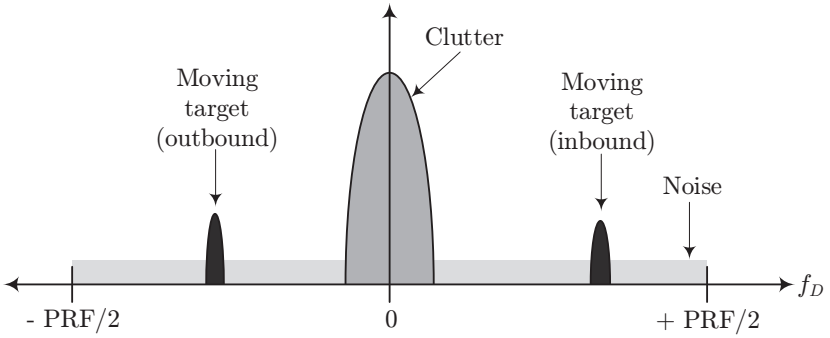

Figure 2.3: Doppler spectrum of M-pulses [3].

In this work, the focus will primarily be on the first three items: targets, clutter, and noise.

The Doppler spectrum of a range bin is the discrete-time Fourier transform (DTFT) of the slow-time data for that range bin. Each of the previously mentioned types of signals will exhibit a different Doppler spectrum. The Doppler spectrum observed at the radar output will be the superposition of the contributions from each signal source.

Consider a stationary coherent radar staring at a certain direction where a particular range bin contains some ground clutter and two moving targets, one approaching the radar and another one receding. Taking the DTFT of that range bin across the slow-time dimension would generate a Doppler spectrum that looks similar to that in Figure 2.3. Because the spectrum of sampled data repeats periodically over the entire frequency band, only the region between $\pm$PRF/2 is shown. From the Doppler spectrum, the following signals are observed:

- White receiver noise spread uniformly across the entire spectrum.
- The spectrum of stationary ground clutter (such as buildings, trees, bushes, etc.) centered around zero Doppler shift. This spectrum can spread if some stationary clutter element has moving parts, such as trees in the wind or fans.
- The two peaks of energy represents the two targets, one at negative frequency, and one at positive frequency. Their position in the Doppler axis is dependent on their individual radial velocities with respect to the radar. Their individual amplitudes relative to the noise are determined by their individual Signal to Noise Ratios (SNRs).

If the target radial velocity v_r is in the interval $(-\lambda\cdot\text{PRF}/4 \leq v_r \leq \lambda\cdot\text{PRF}/4)$, then the Doppler shift will fall in between $\pm$PRF/2 and the Doppler peaks

will indicate the actual radial velocity.

The Doppler shift of targets with a velocity outside this range will alias to an apparent Doppler of $f_D + k\text{PRF}$, where the integer k is chosen such that the result falls in the range $\pm\text{PRF}/2$. The amplitude of the clutter with respect to the noise floor is determined by the Clutter to Noise ratio (CNR).

2.4.2 Doppler Resolution

As discussed in the previous section, the Doppler spectrum of a single range bin is generated by taking the DTFT of multiple pulses over that range bin. The Doppler shift that is caused by a certain moving target will appear as a peak with a limited bandwidth in the Doppler dimension. Having an apparent peak will allow detection. The important question that rises from that is, if there are two moving targets at the same range bin, what is the minimum difference in velocity between the two targets that is required so that their individual Doppler peaks can be distinguished from each other?

The Rayleigh criterion (applied to the Doppler domain) states that two point targets are resolvable when the targets can be separated in Doppler such that the peak of the DTFT of one target falls on the first null of the second target [3]. To apply this statement, let us consider a constant velocity point target illuminated by a radar at a certain range bin over a CPI of M pulses. If the target velocity causes a Doppler shift f_D Hz, then the slow-time received signal at that particular range bin at the output of the coherent detector is

$$s_r[m] = Ae^{j2\pi f_D mT}, \quad m = 0, \ldots, M-1 \tag{2.10}$$

where T is the PRI. The DTFT of Equation 2.10 is given as [3]

$$S_r(f) = A\frac{\sin[\pi(f-f_D)MT]}{\sin[\pi(f-f_D)T]}e^{-j\pi(M-1)(f-f_D)T} \tag{2.11}$$

The magnitude of this equation is plotted in figure 2.4 for the case where $f_D = \text{PRF}/4$ and $M = 20$ pulses. The main-lobe is centered at $f = f_D$ Hz. The radar Doppler resolution parameters that are estimated according to the Rayleigh criterion are:

$$\text{Main-lobe bandwidth} = \frac{1}{MT} = \frac{\text{PRF}}{M} \quad [\text{Hz}] \tag{2.12a}$$

or

$$\text{The width of the main-lobe at } -3 \text{ dB} = \frac{0.89}{MT} = \frac{0.89\text{PRF}}{M} \quad [\text{Hz}] \tag{2.12b}$$

Both parameters are inversely proportional to MT which is the total time of the set of pulses used to make the spectral measurement. Therefore, Doppler resolution increases with increasing the observation time (or increasing M).

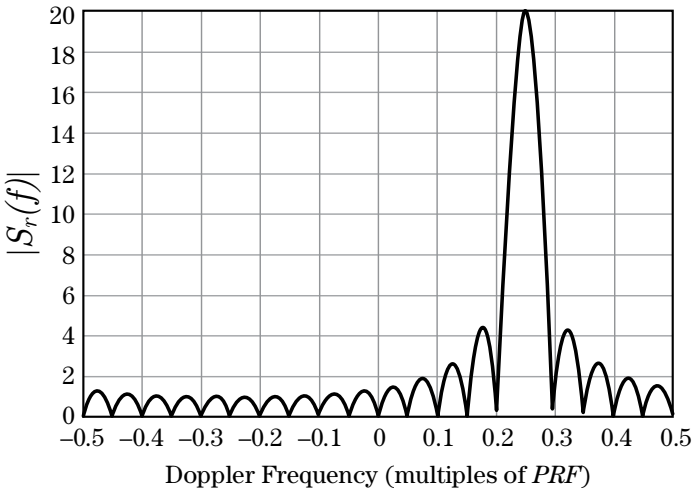

Figure 2.4: Magnitude of the DTFT of a complex sinusoid representing a point target moving at constant velocity such that f_D = PRF/4 Hz and $M = 20$ pulses [3].

2.4.3 Range-Doppler Map

Figure 2.5 shows an example of two targets present in the beam as well as clutter that is distributed among different range bins and Doppler bins. Clutter can be present in all range bins and is centered at zero Doppler shift. A scenario of a radar staring in the direction of two targets present at different range bins moving in different directions is shown in Figure 2.6. This representation of radar signals makes it easy to visualise the target and clutter distribution.

2.5 The Micro-Doppler Effect

Originally, the micro-Doppler effect was introduced in coherent Laser Detection and Ranging systems (LADARs) [1]. LADAR detects the range of an object in a similar fashion as a radar but uses an optical light wave. Also, the concept of coherency is the same as for radar. As coherent LADAR preserves the phase information of the received wave with respect to the transmitted wave, it can measure the velocity of an object from the phase rate of change. LADAR has a greater sensitivity to phase changes. A half-wavelength change in range will cause a 2π change in phase. In the vibration case, if the frequency of vibration is f_v and the vibration displacement is D_v, then the

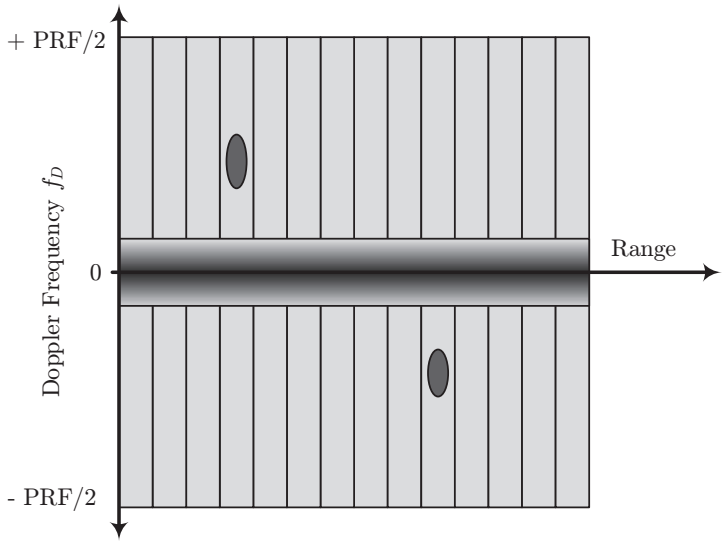

Figure 2.5: 2-D Range-Doppler Spectrum [3].

maximum Doppler frequency variation determined by [1] is

$$\max\{f_D\} = \frac{2}{\lambda} D_v f_v \tag{2.13}$$

As a result, Doppler frequency shifts can easily be detected in high frequency systems, since a very small displacement D_v can cause a large phase change even with a very small vibration rate f_v.

If an object has oscillatory or vibrating parts that create a different motion pattern to the main pattern which moves the object, this motion is called the *micro-motion* [28]. Examples of micro-motion could be the rotating blades of a helicopter and the swinging arms and legs in a walking human which is the subject of interest in this work.

In the Doppler domain, micro-motion modulates extra Doppler shifting about the main Doppler shift. Those extra components are called the *micro-Doppler* components. This modulation enables us to determine the motion pattern of an object of interest and hence assist in identifying this object. This modulation has been discovered as a Doppler audio signal in the early times of radar target recognition [16, 15]. The techniques for time and frequency representation of micro-Doppler as well as how to use them for target classification is still an active subject of research [28].

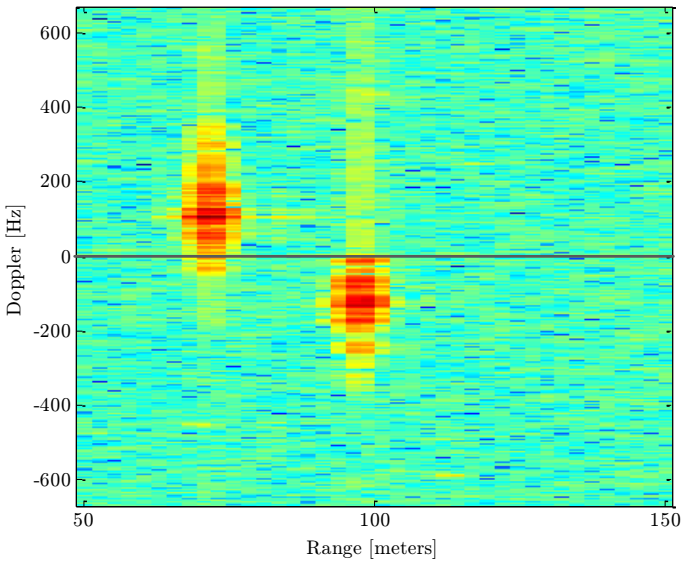

Figure 2.6: 2-D Range-Doppler map.

2.6 Extraction of a Micro-Doppler Signature

The modulation of micro-Doppler components can be extracted from the complex output of the coherent I/Q detector. In addition to the main Doppler shift of the moving target that is normally constant with time, modulation of micro-Doppler will vary with time in accordance to the time-varying dynamics of the target. For this reason, the Fourier transform that is used to extract the range-Doppler spectrum is not suitable to represent this time-varying Doppler information. Therefore, joint time-frequency analysis is required to extract the micro-Doppler modulation.

2.6.1 STFT Based Spectrogram

The most frequently used time-frequency representation of a time-varying signal is the spectrogram. It estimates the change of frequency content of a signal over time. The spectrogram is calculated by using the short-time Fourier transform (STFT). The discrete short-time Fourier transform (STFT) of a signal $x[n]$ is defined as [8]

$$\mathrm{STFT}_x[k,n] = \sum_{r=-\infty}^{\infty} x[r]w[n-r]e^{-j2\pi rk/N} \quad k = 0, 1, \cdots, N-1 \qquad (2.14)$$

where n is the discrete time index, k is the discrete frequency index, and $w[n]$ is a window function.

The STFT can be viewed as the discrete Fourier transform of a signal multiplied by a window function that slides in time. The duration of the window is typically chosen such that the signal of interest is approximately stationary over the duration of the window. A shorter-duration window provides better time resolution but reduced frequency resolution. A longer-duration window provides a better frequency resolution but poor time resolution. This is a classic time-frequency resolution trade-off resulting from using the STFT [7].

The spectrogram is used to extract the pattern of time-varying modulation of micro-Doppler components. The spectrogram of $x[n]$ is defined as the magnitude-squared of the STFT [8]:

$$\text{Spectrogram}_x[k, n] = |\text{STFT}[k, n]|^2 \tag{2.15}$$

Window selection, and the optimum size for the window, will be defined in the next chapter.

2.7 Micro-Doppler Target Signature

The word "signature" is widely used in radar and it refers to various characteristic representations of an object or a process [15]. An example is the overall Radar Cross Section (RCS) plot of an aircraft or a missile which gives it a unique shape in terms of target reflectivity.

In the micro-Doppler domain, a target signature is the spectral image that shows the micro-Doppler characteristics of the target. This image can directly relate to the dynamics of that target. It is a complex-frequency modulation represented in the joint time-and Doppler frequency domain, and it is the distinctive characteristics that give the target its identity [1].

A target can be represented as a set of reflecting point scatterers. Depending on the dynamics of the target, a point scatterer can be regarded as having its own motion. The resultant motion of the point scatterers will give a model of the micro-motion of the overall body of the target. Modelling the micro-Doppler signature of a target is simplified with point scatterers.

2.7.1 Micro-Doppler Signature of a Vibrating Object

A simple motion of a point scatterer can be regarded as an oscillation, vibration, or rotation. The Doppler shift of a vibrating point scatterer is shown in the next paragraph as an example. The same equation has been worked out for other types of motion in [28].

The received Doppler-shifted signal from a vibrating scatterer as a function of time is given in the equation

$$s_r(t) = A \exp\left[j(2\pi f_0 t + \phi(t))\right] \tag{2.16}$$

where A is the amplitude of the received signal, f_0 is the center frequency of the transmitted signal, and $\phi(t)$ is the time-varying phase change of the vibrating scatterer. The time-varying phase $\phi(t)$ of a vibrating scatterer can be modelled as [28]

$$\phi(t) = \beta \sin(2\pi f_v t) \tag{2.17}$$

where $\beta = 4\pi D_v/\lambda$, D_v is the amplitude of the vibration, and λ is the wavelength of the transmitted signal. Substitution of equation 2.17 into equation 2.16 yields

$$s_r(t) = A \exp\left[j(2\pi f_0 + \beta \sin(2\pi f_v t))\right] \tag{2.18}$$

The phase term in the previous equation is a time-varying function. The Doppler frequency induced by the vibration of the scatterer can be represented as

$$f_D(t) = \frac{1}{2\pi}\frac{\mathrm{d}\phi(t)}{\mathrm{d}t} \tag{2.19a}$$

$$= \frac{4\pi}{\lambda} D_v f_v \cos(2\pi f_v t) \tag{2.19b}$$

From the above equation, we note that the micro-Doppler component induced by a vibrating scatterer is a sinusoidal function of time at the vibrating frequency f_v. This component is an important element to simulate the micro-Doppler signatures of complex targets such as human gait. Complex micro-Doppler signatures can also be modelled with other simple micro-Doppler signatures such as rotation, tumbling, and coning. Modelling of micro-Doppler signatures of those types is given in [1] and [28].

2.7.2 Micro-Doppler Signature of a Human

Human motion is a very complex type of motion that involves different types of movement of individual body parts. The way that the human's locomotion is achieved is called the *human gait* [43]. A commonly used method for human gait analysis and recognition is achieved by using sequences of visual images generated by optical equipment. However, visual methods can be affected by distance, light, and environmental conditions. Alternatively, radar has

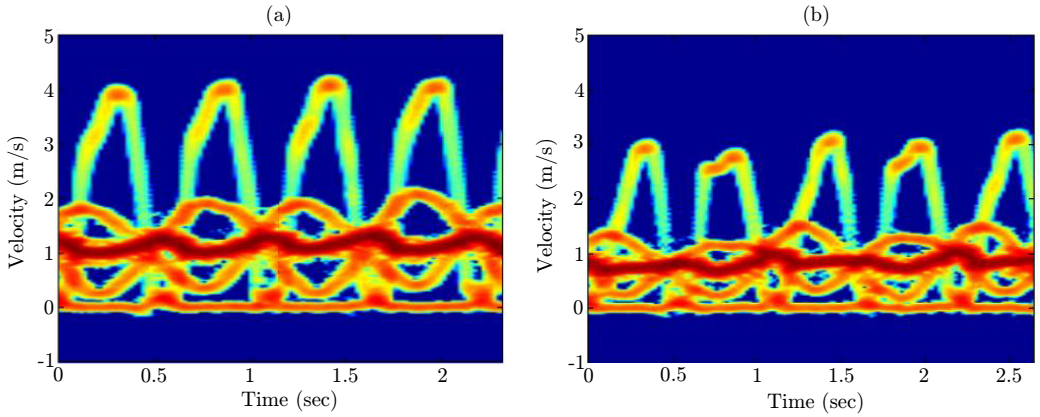

Figure 2.7: Simulated spectrogram of a walking human [32]. (a) Directly inbound. (b) 45° angle inbound.

been widely used as an RF sensor for detection and tracking of targets of interest, having the capability of reaching over long ranges and overcoming the limitations of visual detection systems. Therefore, using radar as a tool to detect humans is a matter of interest.

The motion of a human body can be characterised by a periodic movement of limbs which leads to an articulated locomotion. Walking is a typical example of a human motion which consists of two phases for every gait cycle: a *stance* phase, where one foot is on the ground with a heel strike and a toe off, and a *swing* phase, where one foot is lifted from the ground with acceleration or deceleration [1]. Although this might be the general manner of a human's walk, each individual has different walking characteristics.

The complex human motion can be modelled as a sum of the motion of point scatterers from all body parts. The final Doppler signature is the linear superposition of the Doppler shifts from all the individual point scatterers. There are a number of models for this developed in literature. Such a model will not be re-developed in this work, but one of the available models will be employed for target classification performance measurement as will be shown in chapter 5.

As mentioned earlier in the literature review, models of human micro-Doppler signatures were developed for various reasons: to have a better understanding of the micro-Doppler composition of the signature, to verify experimental data, or to be used as synthetic training data for target classifiers.

2.8 Detection of Targets in Noise and Clutter

Before extracting the signature of a target, it is necessary to detect it first. Extracting the signature is computationally challenging [20]. Hence, it is required to reduce the amount of data for less computation. This can be done by locating the target, then isolating it with a range-gate where only the surrounding information is processed further [30].

Detection is a classical branch of radar. In this section, the part of detection that is required to find a moving target is customised for the purpose of this work.

The main objective of this process is first, to pass on the Doppler spectrum only at the ranges where possible targets are present; and second, to continuously pass it on to the classifier by tracking the targets over range as long as they are present in the beam.

There are various schemes in radar for detection to take place. For our types of targets, it is convenient to use the range-Doppler spectrum as an input to the detection process. The range-Doppler spectrum provides a high SNR and localises the target energy to a detectable peak rising at the associated range and Doppler frequency. To detect a moving target, a suitable threshold, to which each value of the range-Doppler spectrogram is compared, shall be determined.

As is well known in detection theory, each sample from the received signal can be noise-only or a signal corrupted by noise. Given a probability of false-alarm, the detector has to decide for each sample whether a signal is present by comparing the sample to a threshold. The threshold can be either fixed or adaptive. The fixed-threshold technique does not adapt for non-stationarity of the received signal as the false-alarm rate varies over time. Alternatively, an adaptive threshold technique is more likely to perform better. Methods of Constant Flase-Alarm Rate (CFAR) are widely employed in radar to maintain an adaptive threshold [18, 5].

Cell-Averaging CFAR (CA-CFAR) is one of the most common CFAR detectors [4]. A detailed scheme of CA-CFAR is shown in figure 2.8. In this detector, the detection threshold T is given by

$$T = \alpha P_n$$

where α is a scaling factor known as the threshold factor and P_n is the noise estimate. The noise estimate is calculated by simply taking the average of the leading and lagging neighbouring cells around the cell-under-test (CUT)

$$P_n = \frac{1}{N} \sum_{i=1}^{N} x_i$$

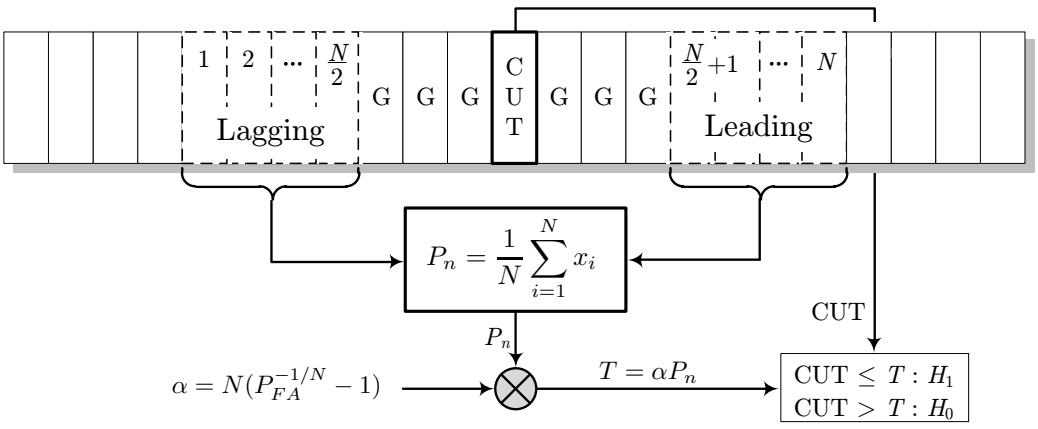

Figure 2.8: CA-CFAR detector [4].

where N is the number of neighbouring cells and x_i is the value of neighbouring cell i. The guard cells are not taken into account as to avoid having part of the signal included in the neighbouring cells which can effect the noise estimate. The threshold factor α is a function of the desired probability of false-alarm (P_{FA}) and the number of neighbouring cells N, such that

$$\alpha = N\left(P_{FA}^{-1/N} - 1\right)$$

2.9 Tracking

The purpose of tracking is to lock the target within a range-gate so that only data that is relevant to the target is processed. As the experimentation data we have contain targets that move in range only, a one-dimensional tracker is sufficient. The basic steps of target tracking will be given in this section. Detailed steps will be explained in the next chapter.

Target tracking consists of the following steps:

1. plot extraction,
2. track initiation,
3. plot-track association, and
4. track deletion.

Plot extraction is the process of identifying the adjacent detections as a single target and replacing them with a single plot. A single plot consists

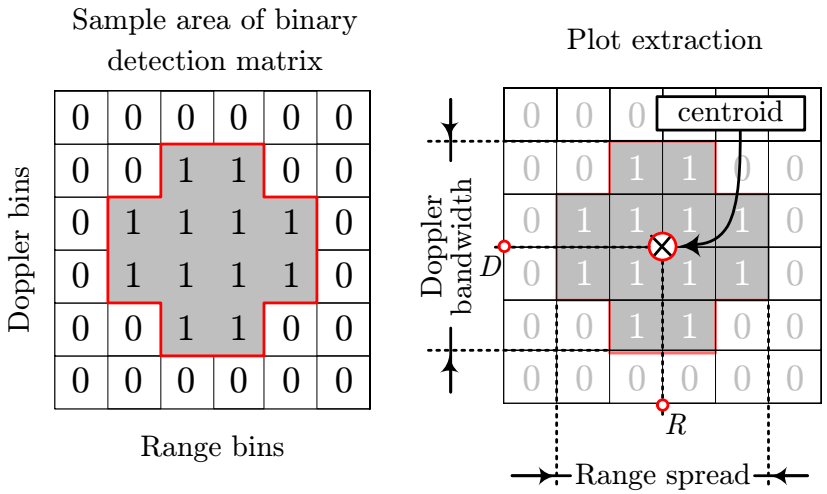

Figure 2.9: Plot extraction from a sample area of the range-Doppler spectrum.

of a measurement of the target's range (R), spatial velocity (v), Doppler shift (D), and direction. These measurements are necessary for the tracking process. Other measurements that are not related to the tracking process but used during feature extraction are: the spread of range sidelobes, Doppler bandwidth, and the size of the range-gate.

Given a binary image representing the detection matrix (see Figure 2.9), there are a few methods that can be used to extract the plots. A well known method is called connected-components labelling or blob-extraction [14]. This process labels adjacent 1's in the detection matrix, which makes it possible to replace them with a single plot. It can also be used to determine the centroid of the detection matrix which makes it possible to locate the plot at the associated range and Doppler shift as shown in figure 2.9.

If plot extraction is carried out for every CPI, plots can be tracked over time. Tracks are initiated for each plot. If a plot from the next CPI falls within close proximity to a track, then this plot will be associated with that track. This process is known as plot-track association [5]. If no plot exists close to a track, then a plot will be declared as missed and a predicted plot will be generated. If the number of misses exceeds a certain acceptable number, then the track will be deleted. As long as the target is being tracked, the data contained within its range gate will be separately processed for target classification. This process will be explained in detail in the next chapter.

2.10 Micro-Doppler Target Classification

After the micro-Doppler signature of a target is extracted, it can be classified. Essentially, target classification can be done by ear: a skilled operator can distinguish one type of target from another by listening to the Doppler extracts [71]. In a sophisticated radar, target classification can be automated. The objective of this work is to develop such a classifier to identify humans.

A typical classification system consists of three major blocks: preprocessing, feature extraction, and classification. The target signature is generated as discussed in the previous sections and then the two-dimensional spectrogram image is provided as input to the feature extractor. A set of features that represent the signature is then passed to a previously trained classifier to identify the target class. Signature extraction was explained in the previous sections. The following two sections explain feature extraction and classification.

2.10.1 Feature Extraction

Feature extraction is an essential process prior to classification. For an input signal represented by a large amount of data, such as an image of a time-frequency distribution of a target signature, it is convenient to decrease this large amount by extracting key features that can best represent the input signature. Recent work in literature shows a variety of methods to accomplish this process. Each one is suitable for one or more than one type of target. The authors of [33] propose a method for extracting seven features based on peak and edge detection in the micro-Doppler spectrogram to discriminate between seven human activities. In [35], a method of extracting three features (symmetry, slope and presence of a middle line) of four types of motion (vibration, coning, tumbling, and rotation) based on the micro-Doppler spectrogram is presented. [30] and [31] employ a simple method for human detection: they extract the human torso contribution by detecting the maximum peaks of the spectrogram. [23] shows how to discriminate between humans and animals using two features, stride rate, which is the rate at which the human take a stride, and another feature that resembles the RCS differences between the main body (torso) and the oscillating parts (appendages) for each target. Another approach is proposed in [37] and [38] which extracts an average frequency difference between the torso and the envelope of the micro-Doppler signature, and uses that to distinguish humans from other types of targets. All the extraction methods mentioned here so far are based on STFT generated signature and applied to a short time frame of the spectrogram (3 to 6 seconds). Other methods that are not based on

STFT can be found in [60], [56], [66], [49], [52], [44], [48], [65], [67], and [70].

In this work, we propose a feature extraction method similar to those presented in [23] and [33]. This method is relatively simple to implement but powerful enough for practical implementation in real-time applications and to detect a variety of targets. The method is based on the periodicity of the target signature, which can be characterised in a spectral map. It is also possible to relate the outcomes of this method, such as velocity and stride-length, to the target's dynamics, as will be shown in section 3.3.

2.10.2 Classification

Given the feature set that represents a certain target signature, it is possible to define the rules to discriminate one type of target from another. It is convenient to design the feature extractor to generate feature sets that can be mapped in a certain space where targets of similar behaviour cluster within the space. Discrimination rules can be applied to create boundaries between those areas and hence discriminate one type of target from another.

There are various classification schemes that can be applied for the purpose of target classification with micro-Doppler signatures. Each scheme varies in performance and accuracy. Target classification using micro-Doppler signature has been studied using various classifiers in literature. In [33] and [34], the authors conducted the classification task with Support Vector Machine (SVM) and Artificial Neural Network (ANN) based classifiers. The SVM is found to perform slightly better than the ANN for a set of six features and an output of seven classes. In [35], a comparison test was performed on five types of classifiers: Bayes Linear Discriminant Classifier (LDC), Bayes Quadratic Discriminant Classifier (QDC), k-Nearest Neighbour (k-NN), SVM, and ANN. Those classifiers were tested against four classes of motion: vibration, rotation, coning, and tumbling. All classifiers are found to perform well, except for a considerable error rate of 12% using the ANN. However, the authors of [24] do a classification performance analysis of three types of classifiers: Support Vector Machine (SVN), Artificial Neural Network (ANN), and Nearest Neighbour (NN). The classifiers were tested against the same types of motion given in the previous paper and conducted a similar feature extraction method. The results shows slightly better performance using the ANN as opposed to the other classifiers.

It is important to note that the previous studies employed similar types of classifiers but certainly with different configurations, hence the variety of their results. But most of the studies show that, if the target features are well defined, they will be easily recognised, regardless of which classifier is used.

In this work, a neural network based classifier will be designed to perform the classification task. This design choice was made upon earlier examination of the proposed feature extraction method with an A-NN classifier which has shown an acceptable performance. This increased the confidence that the proposed feature-set is defined well enough for any classifier to be suitable.

The following section introduces the common neural network configuration that is found to be suitable for micro-Doppler based target classification, along with the training mechanism. The chosen configuration is the multilayer feed-forward perceptron with back-propagation training algorithm [9]. The design procedure will be shown in the next chapter.

2.10.3 Overview of ANN Classifiers

Single-Neuron Model

Before we begin discussing the multilayer perceptron (MLP), a short overview of a single neuron is given[1].

A multi-input neuron is shown in figure 2.10. This neuron computes a weighted sum of its R inputs, $p_1, p_2, \ldots, p_R$. The summation n (the net input) goes into a transfer function f, also known as the *activation function*, and generates a scalar output a. If the sum n is above a certain threshold b, then $a = 1$, otherwise $a = 0$. Mathematically, this can be written as:

$$a = f\left(\sum_{j=1}^{R} w_j p_j + b\right) \tag{2.20}$$

where $f(\cdot)$ is an activation function (e.g. a step function at 0), and w_j is the weight associated with the jth input. The threshold b (also known as the *bias*) is often considered as another weight $w_0 = b$ attached to the neuron with a constant input $p_0 = 1$. This equation can be rewritten in a matrix form:

$$a = f(\mathbf{W}\mathbf{p} + b) \tag{2.21}$$

where the matrix $\mathbf{W}$ is the weighting matrix, with only one row in the single neuron case. There is a variety of activation functions that can be used that are suitable for different applications. The most frequently used function, other than hard-limit threshold function, is the sigmoid function defined as

$$f(n) = \frac{1}{1 + e^{-n}}$$

The two functions are shown in figure 2.11 and 2.12

[1] This section follows the description in [9].

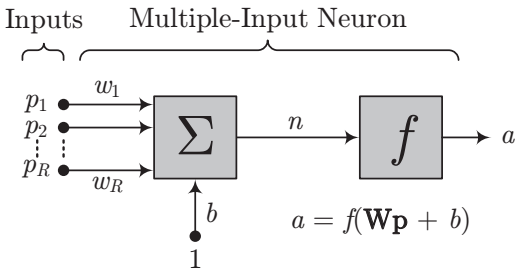

Figure 2.10: Single layer perceptron.

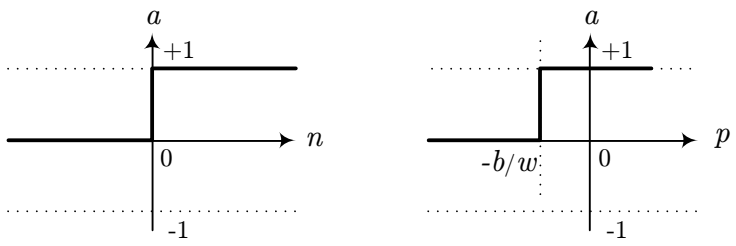

Figure 2.11: Hard-limit activation function.

Learning with the Backpropagation Algorithm

The learning procedure in ANNs networks can be seen as a process of updating the network architecture and connection weights so that it can efficiently perform a specific task. The network must learn the connection weights from available training data. Its performance improves over time as the weights in the network are iteratively updated.

To understand the learning process, it is important to have a model of

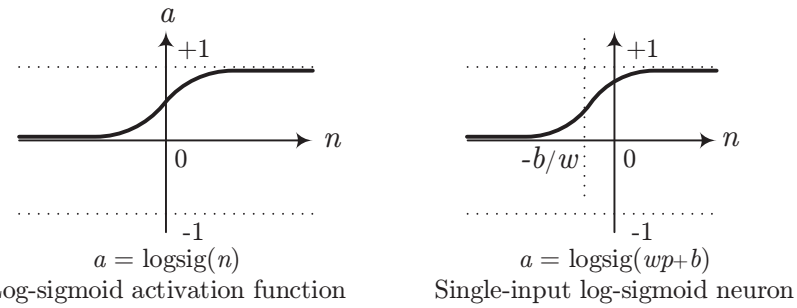

Figure 2.12: The log-sigmoid activation function.

the environment in which a neural network operates. In other words, it is important to know what information is available to the network. This model is referred to as the *learning paradigm*. Secondly, it is important to understand how the weights are updated and which learning rule governs the updating process. The learning rule refers to the algorithm or procedure in which rules are applied when calibrating the network weights.

There are three main learning paradigms presented in literature: supervised, unsupervised, and hybrid. In supervised learning, as will be employed in this work, the training procedure is carried out while the network is provided with the correct output result $\mathbf{a}$ for every input $\mathbf{p}$. The weights $\mathbf{W}$ are calibrated to allow the network to give outputs as close as possible to the known correct desired outputs. On the other hand, unsupervised learning does not require specification of desired outputs associated with each input training set. Hybrid learning combines the previous two learning paradigms. Four learning rules are commonly used: error correction, Boltzmann, Hebbian, and competitive learning [42]. For simplicity, the error correction rule is sufficient for our work.

In the supervised learning paradigm, the network is given a desired output for each input set. During the learning process, the actual output a generated by the network may not equal the desired output d. The basic concept of error-correction learning rules is to use the error value $(d-a)$ to calibrate the connection weights in order to gradually reduce this error. The perceptron learning rule is based on the error-correction rule. To show this concept, let us consider a perceptron of a single neuron with R adjustable weights, $w_1, w_2, \ldots, w_R$, and bias b as shown in figure 2.10. Given an input vector $\mathbf{p} = [p_1, p_2, \ldots, p_R]$, the net sum of the neuron is

$$n = \sum_{j=1}^{R} w_j p_j + b$$

If we employ a step function as the activation function, the output of the perceptron is $+1$ if $n > 1$ and 0 otherwise. In a two-class classification problem, the perceptron assigns an input set to one class if $a = 1$ and to the other class if $a = 0$. The linear equation

$$\sum_{j=1}^{R} w_j p_j + b = 0$$

defines the decision boundary that halves the space. The perceptron learning algorithm can be summarised as follows:

1. Initialise the weights and bias to small random numbers.

2. Present a pattern vector $\mathbf{p} = [p_1, p_2, \ldots, p_R]^T$ and evaluate the output of the neuron.

3. Update the weights according to

$$w_j(t+1) = w_j(t) + \eta(d-a)p_j$$

where d is the desired output, t is the iteration number, and η $(0 < \eta < 1)$ is the gain (step size).

Learning occurs only when the perceptron makes an error. It has been proved that, when training sets are drawn from two linearly separable classes, the perceptron learning procedure converges after a finite number of iterations [9], [42]. This idea is known as the *perceptron convergence theorem*. The backpropagation learning algorithm is also based on the error-correction rule.

Single-layer Perceptron

A single-layer network of S neurons is shown in figure 2.13. The layer includes the weight matrix $\mathbf{W}$, the summers, the bias vector $\mathbf{b}$, the activation function blocks and the output vector $\mathbf{a}$. It is common for the number of neurons in a single layer not to be the same as the number of inputs. In other words, $S \neq R$. It is also common for the activation functions not to be the same. A single-layer network with activation functions of either a hard limit or a sigmoid is called a single-layer *perceptron*.

Multi-layer Perceptron

A multi-layer network is shown in figure 2.14. Each layer now has its own weight matrix $\mathbf{W}$, its own bias vector $\mathbf{b}$, a net input vector $\mathbf{n}$ and an output vector $\mathbf{a}$. A layer of which the output is the network output is called an *output layer*. The other layers are called *hidden layers*. The network shown here has an output layer (layer 3) and two hidden layers (layers 1 and 2).

Multi-layer perceptrons commonly employ the backpropagation algorithm for calibrating their weights [9].

Design Issues

Many issues arise when designing multi-layer perceptrons, such as:

- how many layers are needed for a given task,
- how many units are needed per layer,

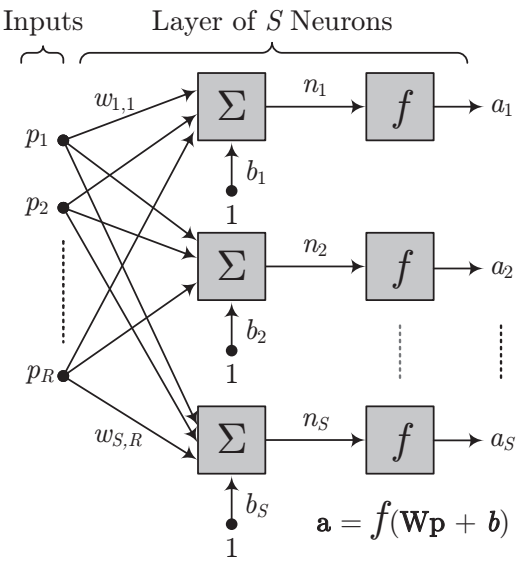

Figure 2.13: S-neuron single-layer perceptron.

- how efficient the network performs on data that is not included in the training set (its ability to generalise), and
- how large the training set should be for good generalisation.

Although the multi-layer feed-forward networks which use backpropagation have been widely used for classification applications, many design parameters, such as weights and number of layers, still take the trail-and-error method to determine their values for optimum results. Only loose guidelines are provided in the existing theoretical results for choosing these parameters [42].

Derivation and implementation steps of the backpropagation algorithm for the feed-forward network are found in [9] and [42].

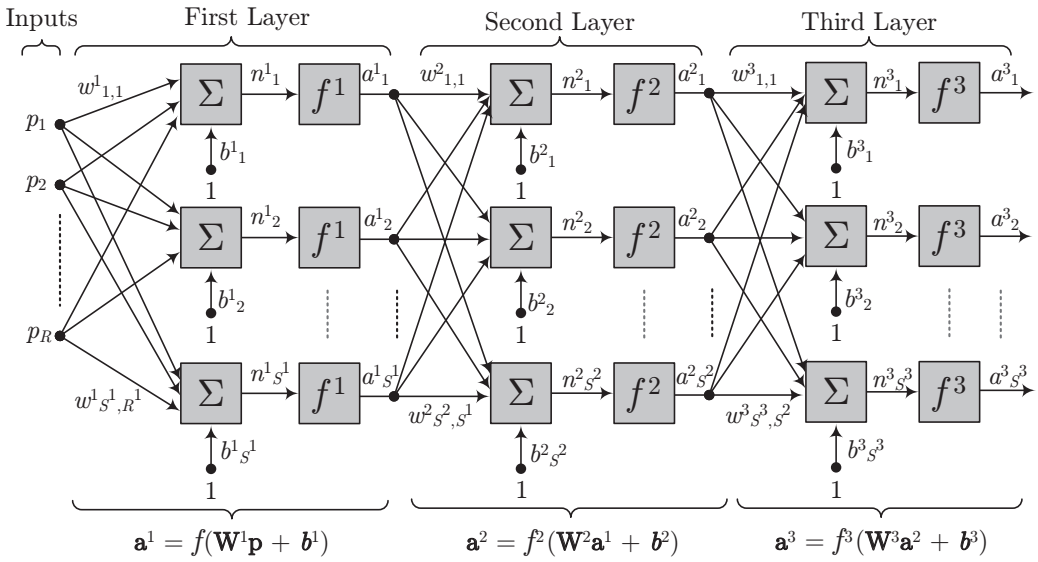

Figure 2.14: The multi-layer perceptron.

Chapter 3

System Design

3.1 Introduction

In this chapter, the design of the Radar Human Detector as well as the concepts and methods underlying the detection process are discussed. The chapter will start by giving an overview of the operating scenario of the radar where the human detector can be employed, along with the operational assumptions. The overall objectives and concept diagram of the system are given in section 3.3. Extraction of the micro-Doppler signature of the target is detailed in section 3.6. Section 3.7 will explain the method for extracting features from target signature. Finally, section 3.8 details the development of two types of classifiers.

3.2 Radar Operational Scenario

The capability of detecting humans can be applied in various applications such as protecting a border or facilities from possible human presence. For the radar to use the designed human detection system, the following assumptions are made:

1. It is assumed that the radar is able to detect the presence of moving targets within its detection range. Radars with Doppler or MTI detection capability can provide first detection while operating in a full-scanning or a sector-scanning modes.

2. Once the detected targets are displayed on the radar screen, we assume that the operator is given the option to direct the antenna beam at the target of interest to evaluate the target by initiating the human detection process. An example is given in Figure 3.1.

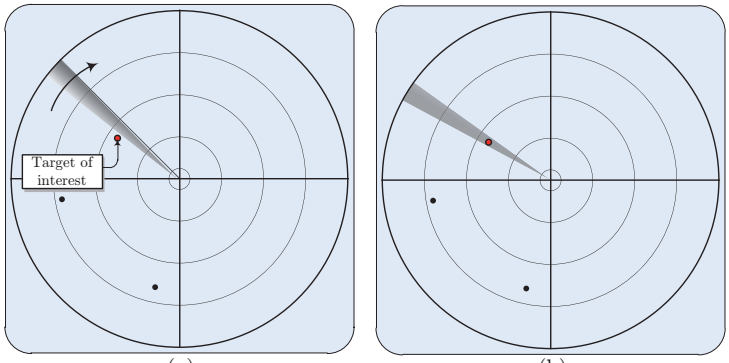

Figure 3.1: Typical scenario of a surveillance radar: (a) Detection displayed in Scanning Mode. (b) Staring at the target of interest.

3. While the target is being detected in the beam, we assume thatit will be isolated and tracked within a range-gate that is centred at the range of the target. The range-gated data will then be sent to the human detector to evaluate the presence of humans.

4. The human detection algorithms developed in this work are specifically applied and tested with a low-power FMCW radar (RSR940). However, those algorithms can easily be modified to work in other types of radars with Doppler capability. An overview of the RSR940 Radar System is given in chapter 4.

   It is more likely that the radar can efficiently evaluate the target if it moves directly inbound towards the radar, or directly outbound away from the radar. As will be shown in our tests in chapter 5, radial motion inside the beam produces the highest Doppler content. Micro-Doppler signatures that are obtained from tangential movement across the beam, or crossing the beam with an angle, will be examined in this work, although they might not be suitable for human detection.

3.3 System Design

The overall concept diagram of the human detection system is shown in Figure 3.2. Radar input data are samples received from the ADC module in the signal processor. Those samples are the time-domain complex samples of the output of the coherent detector. In the second block, the first detection process is performed. The range gated data of each individual target in the beam is generated. In the third block, the human detection process

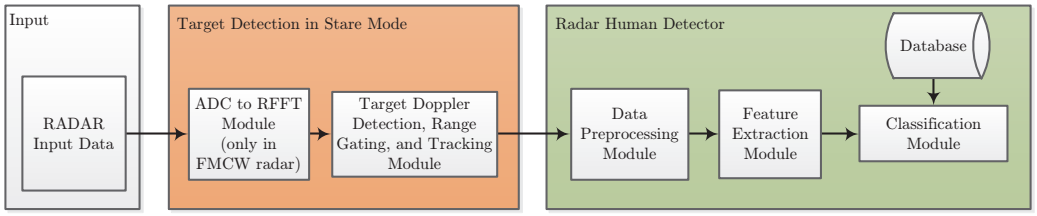

Figure 3.2: Overall system concept diagram.

is performed. This process begins by generating the target micro-Doppler signature by means of joint time-frequency analysis in the data preprocessing module in a suitable manner for feature extraction. In the feature extraction module, a periodicity-based method is performed to extract eight features. Finally, those features are used to perform target classification and the second detection process takes place.

The following sections explain the design of each individual block.

3.4 System Input Data

A block diagram of the input data interface that is used for this work is shown in Figure 3.3. As it is the case for most conventional radars, the radar waveform is generated by the synthesiser and sent to the transmitter for frequency up-conversion and filtering of spurious frequency components. The signal is amplified and sent to the transmitting antenna. The echoes from the transmitted signal are received by the receiver's antenna, then down-converted to baseband. The baseband signal are sampled by the Analogue to Digital Converter (ADC). The samples are captured and sent through the radar slip-ring via a high-speed Ethernet link to the computer.

Two input modes are defined for this system:

1. **Real-time live streaming**
   In this mode, the radar is in operation. The received signals are sampled and digitised in the radar signal processor then streamed through the slip-ring via high-speed Ethernet to a PC where the detection processes take place. Also in this mode, the radar can be used to record and store data on the hard drive, as shown in Figure 3.3.

2. **Real-time streaming of recorded data**
   In this mode, the data is streamed via a data playback tool that can read previously-recorded data and stream it to the system in an equivalent mechanism to the previous mode. The real-time tests for the

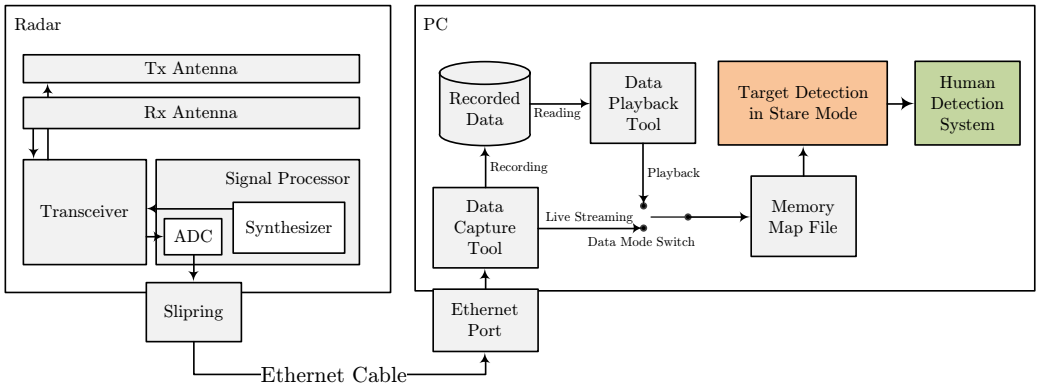

Figure 3.3: Input data to the human detection system.

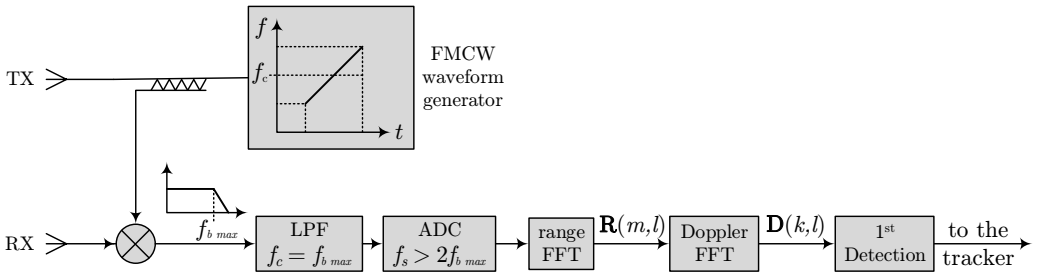

Figure 3.4: Simple block diagram of an FMCW radar system.

Human Detection System will only operate in this mode as it is designed to be equivalent to the real-time operational radar.

3.5 Target Detection and Tracking

In this system, the detection and tracking of moving targets are required for two reasons: firstly, to extract only enough data needed for preprocessing, and secondly, to separate one target from another so that each target can be evaluated and classified individually. The required steps to extract the individual target's data from the entire data are as follows:

1. Generation of a range-Doppler matrix.
2. Clutter suppression.
3. Suitable estimation of the detection threshold.
4. Detection of returns above the threshold.

5. Plot extraction and estimation of basic target information.

6. Track initiation and plot-track association.

7. Track maintenance and generation of associated range gated data.

Those steps are detailed in the following sections. It is important to note that this part of the system design is not the primary focus of this work but a necessary step before carrying out the classification process.

3.5.1 Range-Doppler Matrix

Summary of variables

N	=	Number of samples in time-domain signal.
M	=	Number of sweeps (or pulses). Also known as the burst size.
n	=	The time sample index.
m	=	The sweep number (or pulse-number).
NFFT_R	=	Number of RFFT points.
NFFT_D	=	Number of DFFT points.
L	=	Number of range bins.
l	=	Range-bin index.
δ_R	=	Range resolution [m].
K	=	Number of Doppler bins.
k	=	Doppler-bin index.
δ_D	=	Doppler resolution [Hz].
SRI	=	Sweep repetition interval.
SRF	=	Sweep repetition frequency.
$R(l)$	=	$(1 \times L)$ Range vector.
$\mathbf{R}(m, l)$	=	$(M \times L)$ Range-burst matrix.
$\mathbf{D}(k, l)$	=	$(K \times L)$ Range-Doppler matrix.

Range-FFT (RFFT)

For different radars, range can be resolved with various methods. In FMCW radar, the range to a target can be obtained from the difference in frequency between the transmitted sweep and the delayed echo reflected from that target. Figure 3.4 shows a simple block diagram of an FMCW radar system. For every sweep, the output of the mixer is a multi-tone signal Each tone corresponds to the range of the target. The higher the tone, the farer the target. The highest tone at the output of the mixer is designed in such a way to correspond to the maximum instrumented range of the radar. To

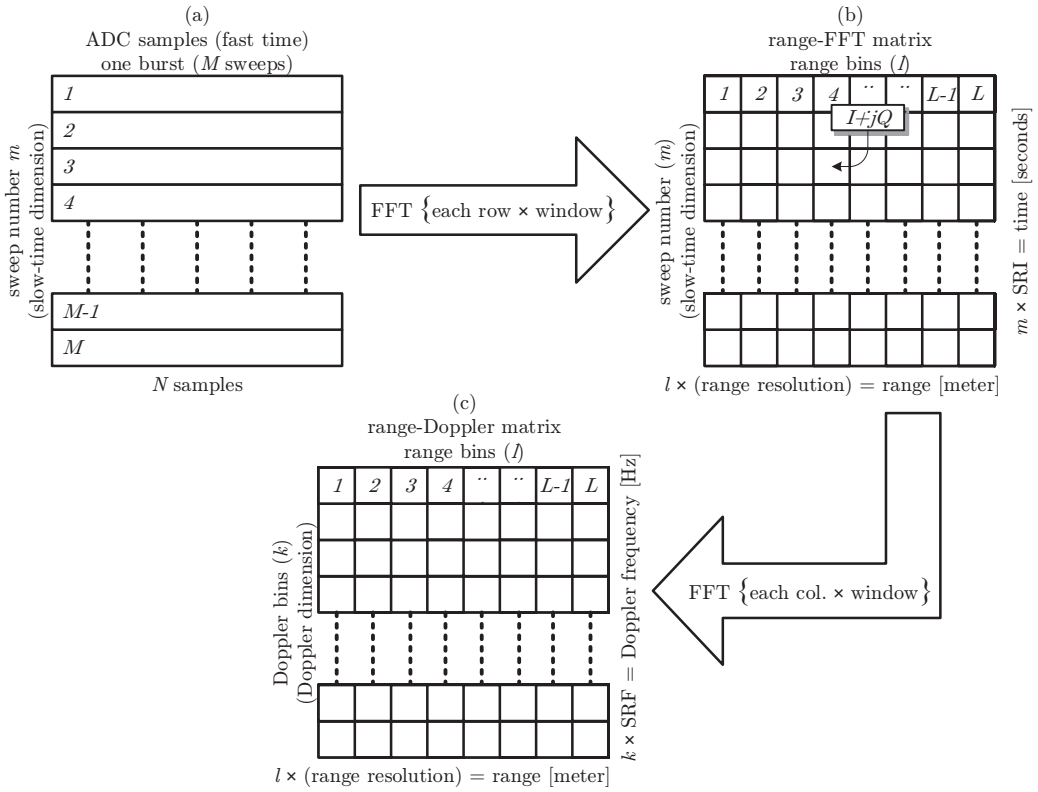

Figure 3.5: Resolving range and Doppler from raw-ADC samples: (a) N-samples of multiple sweeps. (b) Range-FFT matrix **R**. (c) Range-Doppler matrix **D**.

allow for detection, the multi-tone signal, once sampled, is represented in the frequency domain. If a target is present at certain range, a peak will rise at the tone-frequency of the corresponding range. The peak corresponds to the amplitude of the reflected signal from the target. Additionally, the phase of tone can be obtained. This translation of range from time-domain to frequency-domain is known as stretch-processing [3]. Range-FFT (RFFT) is a common method of performing stretch-processing in FMCW radars [6]. Figure 3.5 shows the process of resolving target range with RFFT.

Each multi-tone signal is sampled to N samples. The duration of N samples equals the sweep-repetition-interval (SRI). Range-FFT is produced by computing the FFT of those samples (row-FFT of Figure 3.5a), providing a vector of L elements. Each element is a complex number representing the amplitude and phase. Example of an output of a single sweep range vector is shown in Figure 3.6. Example output of a Range-FFT, or target range over 30 seconds (40,000 sweeps) is given in Figure 3.7.

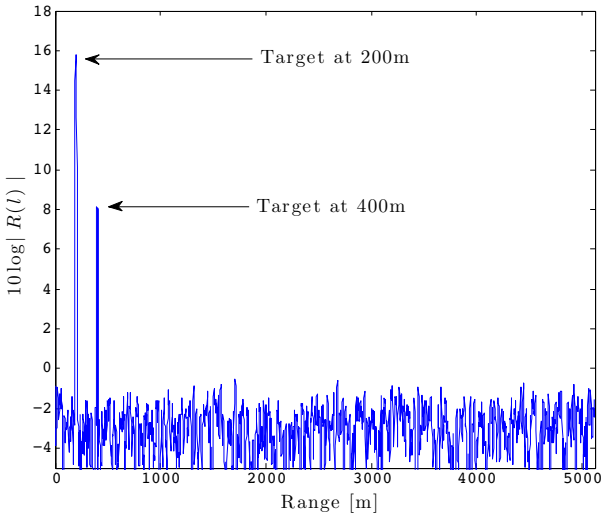

Figure 3.6: The magnitude of a range-FFT vector R. Example of range-FFT output of a single sweep showing two targets.

Doppler-FFT (DFFT)

As discussed in the previous chapter, moving targets cause a Doppler shift in the returned signal. This shift can be extracted from the change in phase.

The benefit of using Doppler for detection is to be able to detect moving targets from clutter, therefore enhancing the detection process. The Doppler information that is required for detection can be obtained with an extra process called Doppler-FFT. This process provides not only the range information of the targets, but also the Doppler information for each range-bin. First, a number of sweeps are stacked in rows defining a burst. The target is expected to slightly move between one sweep and the next. The Doppler shift in the returned signal will cause a phase-change in the corresponding target range-bin. The burst size is measured in number of sweeps (pulses in the case of pulsed-radar).

The Doppler information can be extracted by taking the FFT across the slow-time dimension of the range-FFT matrix for each range-bin (each column in Figure 3.5.b). The intensity-image of the absolute value of the range-Doppler matrix is called the range-Doppler map. It is used to monitor the radar returns with respect to range and Doppler shift. Stationary clutter will be concentrated in the zero-Doppler line with its corresponding range. Only moving targets are spread away from the zero-Doppler line. Targets that are approaching the radar will have a positive Doppler shift and those that are departing away have a negative Doppler shift. Depending on the

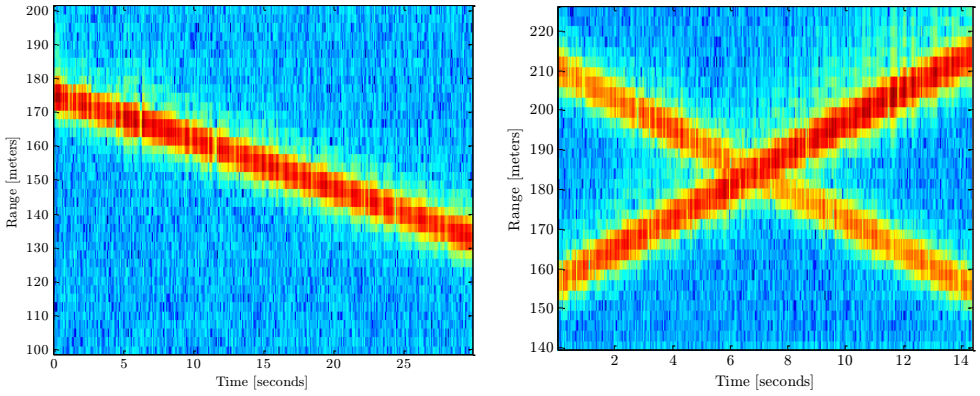

Figure 3.7: Magnitude intensity image of a range-FFT matrix. The time-axis $= m \times$ SRI. (a) One person walking inbound. (b) Two people walking inbound and outbound.

radar range resolution, targets can be separated in range. Targets that are in the same range bin will interfere with each other unless the two are moving in opposite directions to one another, in which case they can be separated in the Doppler domain. Figure 3.8 shows an example of a range-Doppler map of two targets moving in opposite directions.

3.5.2 Detection of Moving Targets

A simple detector is designed to detect moving targets from the range-Doppler matrix. A basic cell-averaging CFAR (CA-CFAR) is employed to adapt the detection threshold for every burst and every Doppler bin. The outcome of the detector is a binary matrix of the same size as the range-Doppler matrix with the digit "1" corresponding to values above the threshold and "0" corresponding to values below the threshold. Figure 3.9 shows an image of the detection matrix of the two targets shown in Figure 3.8.

3.5.3 Target Tracking

The objective of tracking, as was discussed in the previous chapter, is to identify the present targets with tracks, lock each track with a range-gate, and pass on the range-gated data to the classification process.

Firstly, the detection matrix is translated to plots. Each plot corresponds to the area of binary detections of a single target. Plots are generated through a standard process called connected-components-labelling, where each area

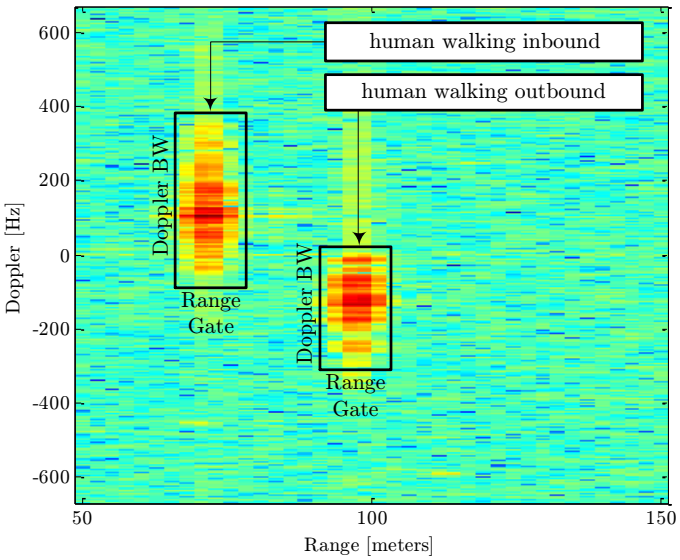

Figure 3.8: Range-Doppler map of two humans walking inbound and outbound.

of detections is represented by a single point which is the centroid of that area. Plots are generated for every CPI (i.e. for every burst).

Secondly, the tracking process is initiated with the first available plots. Each plot is assumed to be the beginning of a track. Tracks are updated for every burst in the following manner:

- A tracking window is associated to each track. The size of that window is a function of the target speed.
- New plots are examined. If a plot falls within the tracking window of a track, this plot is associated to that track. Otherwise, the track will be updated with a missing plot and the new plot will initiate a new track.
- If the number of missing plots for a given track exceeds a certain value, the track is deleted.
- As long as the target is tracked, the range bins that are bounded within the track range gate are passed to the classification preprocessor. An example of range-gated data is shown in Figure 3.11.

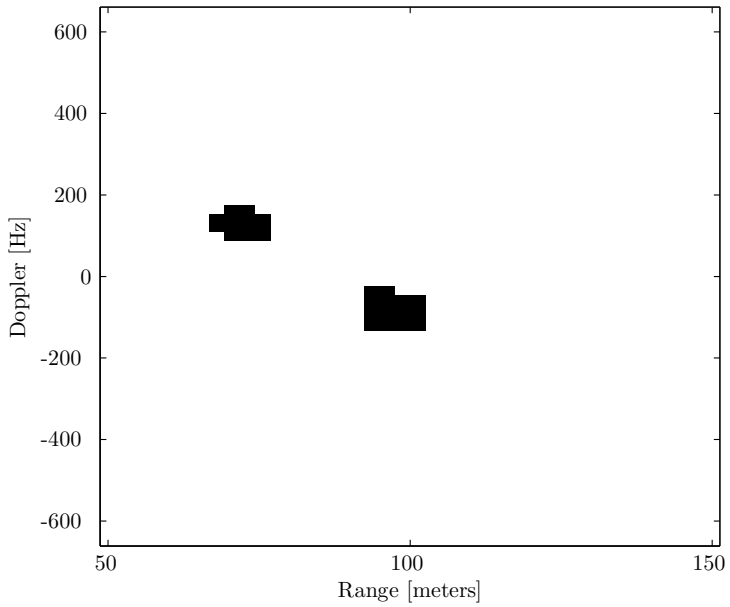

Figure 3.9: Detection map of two humans walking inbound and outbound.

3.6 Data Preprocessing

The objective of data preprocessing is to represent the data in a form suitable for feature extraction. The conventional method that is commonly used to represent the micro-Doppler target signature is based on time-frequency analysis.

STFT (Spectrogram)

The spectrogram is a straightforward method to represent the variations of a signal over time and frequency. Given a target's range-gated data, the spectrogram is computed for every burst, as shown in Figure 3.12, in the following manner

- For each range bin, the spectrogram is computed using the discrete short-time Fourier transform given by equation 2.15.
- As the returned energy from the target occupies more than a range bin, the individual spectrograms are added together to form an integrated spectrogram of the target.

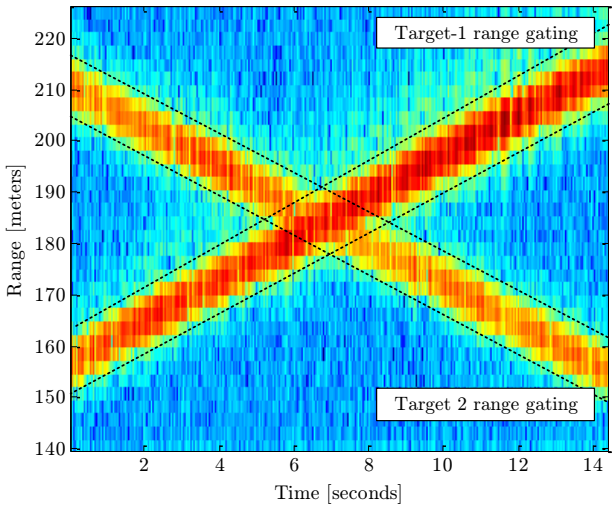

Figure 3.10: Range gating.

An example of an image of a walking human STFT-based signature is shown in Figure 3.14.

3.7 Feature Extraction

3.7.1 Human Signature Characteristics

Figure 3.13 shows a typical micro-Doppler signature of a walking human. The physical parameters of a walking human signature are shown in Figure 3.14. The objective is to extract some features that are in direct relation to

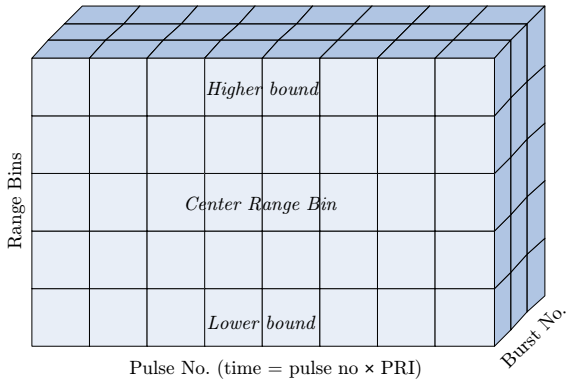

Figure 3.11: Target Range Gated Data.

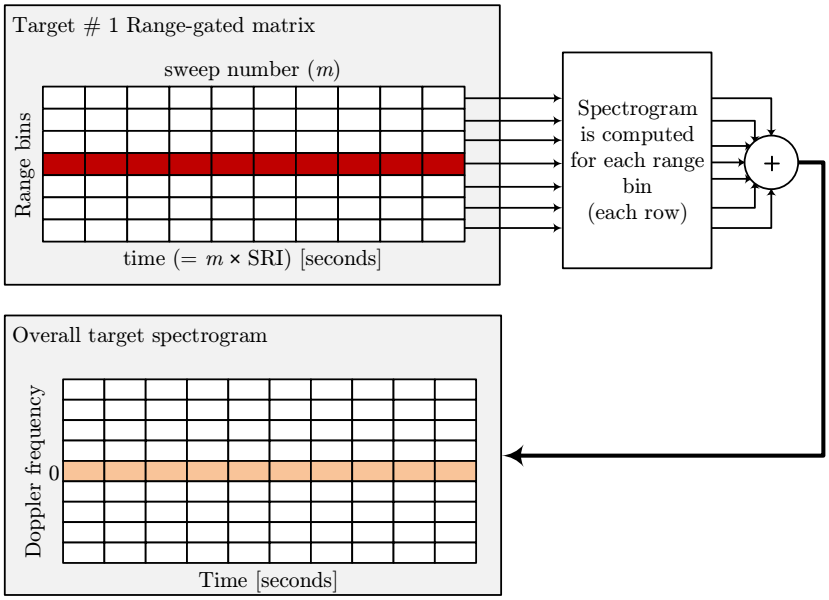

Figure 3.12: Target spectrogram over an entire range gate

these parameters.

The parameters that are marked with numbers in Figure 3.14 are defined as follows:

1. **Main Doppler line**: This component contains the highest Doppler energy from the target. If the target is a human, it results from the constant (and slightly swinging) movement of the torso.

2. **Gait cycle**: The time between two alternating steps.

3. **Period**: The time between two peaks in the upper or lower envelope. In the case of human targets, it is called the step period.

4. **Micro-Doppler bandwidth**: The entire range of Doppler variations of the target. In the case of humans, it is an indication of the swinging velocity of the arms and legs.

5. **Main Doppler line bandwidth**: This is the bandwidth of the Doppler signal without micro-Doppler modulation.

6. **Phase variations**: These are the phase offsets between micro-Doppler envelopes (i.e. the variation in the time between the different micro-Doppler envelopes crossing the main Doppler line).

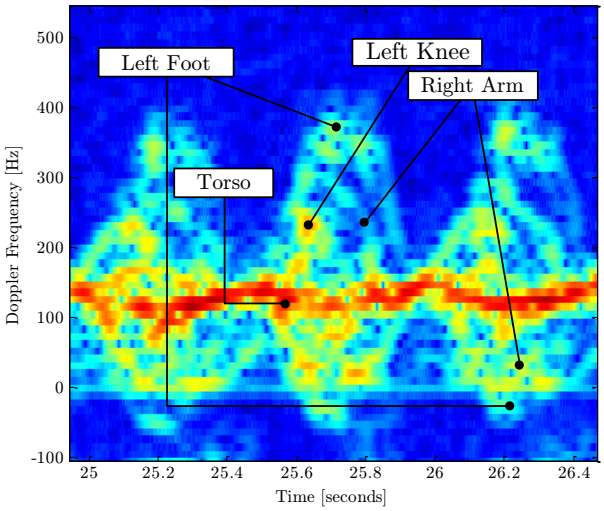

Figure 3.13: Micro-Doppler human signature decomposition (three steps).

7. **Zero-Doppler line**: The Doppler line around which the energy of stationary targets and clutter resides.

3.7.2 Gait-Doppler Map

A simple method to measure the periodicity of the target's signature is to take the FFT across the time axis [23]; this is performed by computing the row-FFT of a short time frame of the spectrogram image, such as the one in Figure 3.13. The minimum duration of the frame is chosen in such away to provide more than one gait cycle. The more gait cycles, the lower the side-lobes of the row-FFT. A feature extraction mechanism is developed in this work based on that method with a number of improvements:

1. We propose a normalisation process that maintains the same results for different time frames of the spectrogram. Without normalisation, the different time frames of the same target will give different features which will lead to misclassification.

2. This method is employed in real time.

3. Additional features are added to the feature-set.

The output image of the spectrogram row-FFT, such as the one shown in Figure 3.15, is titled here as the Gait-Doppler map, where the x-axis (gait-frequency) is the frequency of which the different body parts oscillates in

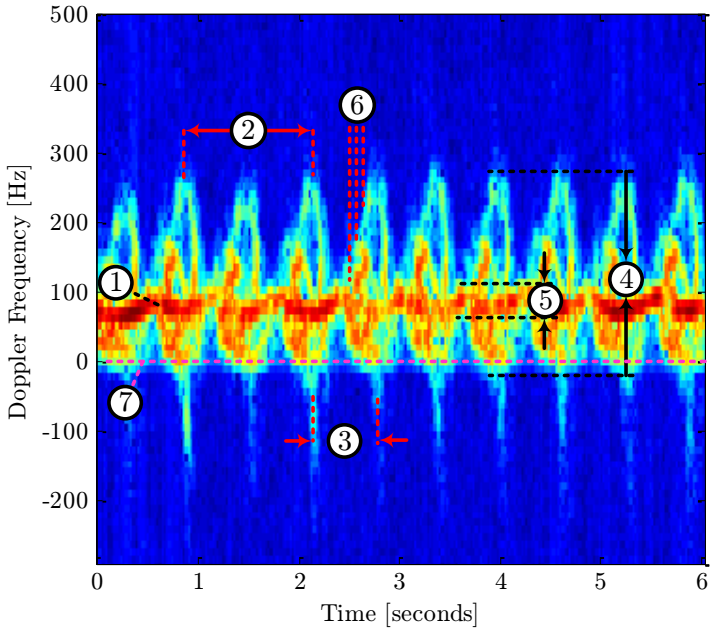

Figure 3.14: Spectro-temporal features as observed for a human target.

Doppler. The intensity (in colour) represents the Doppler energy decomposition of the object's parts with micro-motion. Figure 3.15 shows an example of the row-FFT output of the spectrogram image extracted from the target in Figure 3.14.

From that image, the following peak amplitudes are observed:

1. **Low gait frequency component**: The constant velocity of torso as well as its slight oscillation will result in a peak close to DC in the gait frequency axis.

2. **Periodic motion of micro-Doppler components**: In the case of a human, this results from the periodic motion of arms and legs that is modulated around the main Doppler line.

3. **Extra gait harmonics**: These are the 2^{nd} and 3^{rd} harmonics of the periodic motion of the arms and legs.

3.7.3 Feature Extraction Mechanism

A time-framed window of the target spectrogram will be processed for feature extraction. The time length of the window is chosen just short enough for the

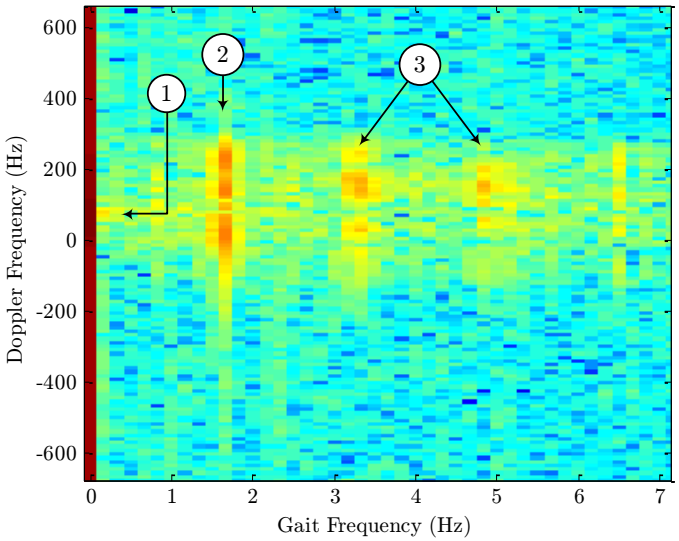

Figure 3.15: Gait-Doppler map (row-FFT of the spectrogram).

row-FFT to resolve the periodicity to significant peaks in the gait-Doppler map.

In the case of humans, a relationship between the required time length of the spectrogram time-frame and the velocity of the target can be obtained. As will be shown in a later chapter, the faster the target is moving, the faster the hands and legs are swinging. Hence, short gait cycles and a shorter time frame is needed.

Given the gait-Doppler map for one target, and the main parameters defined in section 3.7.1, the following features are defined:

1. **Target average radial velocity** (v_{av}): This value can be obtained from the average Doppler frequency f_{av}. One way to find f_{av} is to calculate the average of two Doppler frequencies at which the peak energy from the torso occurs. The peak energy can be obtained from the first two gait-frequency bins (the first two columns) from the gait-Doppler map. Figure 3.16 illustrates this process. Both curves are extracted from the gait-Doppler map in Figure 3.15. The upper curve is a plot of the DC gait-frequency bin (1^{st} column) and the lower curve is a plot of the adjacent gait-frequency bin (2^{nd} column). Both peaks correspond to the Doppler energy from the torso. In this example, both peaks happened to have the same Doppler frequency of 83.75 Hz. The average radial velocity of the target can be obtained by substituting

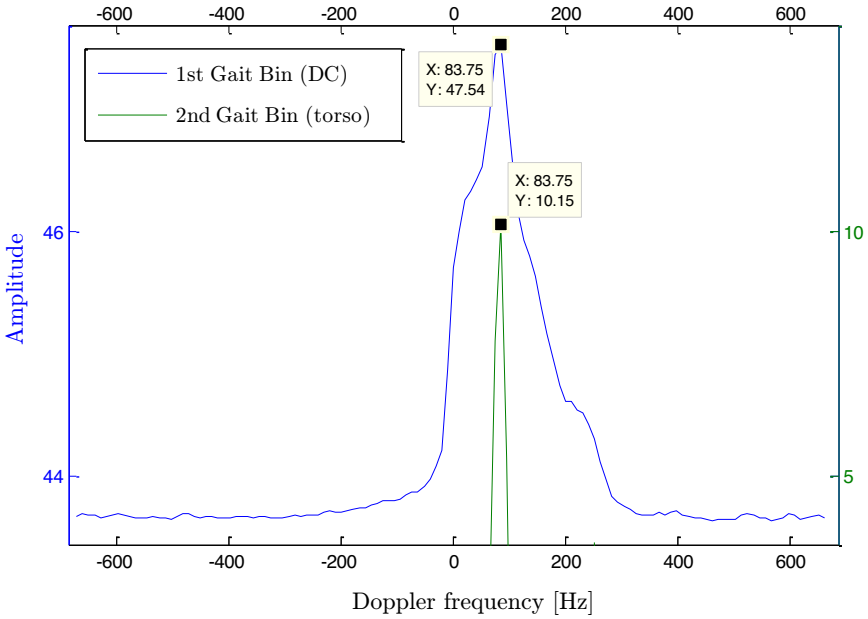

Figure 3.16: Torso signal intensity across the Doppler axis.

f_D in the equation:

$$f_D = f_0 \frac{2v_{av}}{c} \quad \rightarrow \quad v_{av} = 2c\frac{f_D}{f_0} \quad [\text{m/s}] \tag{3.1}$$

2. **Micro-Doppler bandwidth** ($B_{\mu D}$): This value can be estimated from the range-Doppler map (e.g. Figure 3.8). This feature gives an indication of the overall variations of swinging velocities.

3. **Stride Length** (L_s): Stride is found to be a fundamental feature that distinguishes walking beings from other objects with a micro-Doppler signature, as will be shown in the results. Stride is the length of one step, which can be obtained by finding the gait frequency f_m at which the fundamental gait component occurs, then substituting that in the formula

$$L_s = \frac{v_{av}}{f_m} \qquad [\text{m}] \tag{3.2}$$

4. **Gait-harmonic frequency ratios** (β_1 and β_2): This is an indication of the range in which the gait frequencies' harmonics fall. The significance of this feature is to restrict the peak-detector to detect the right

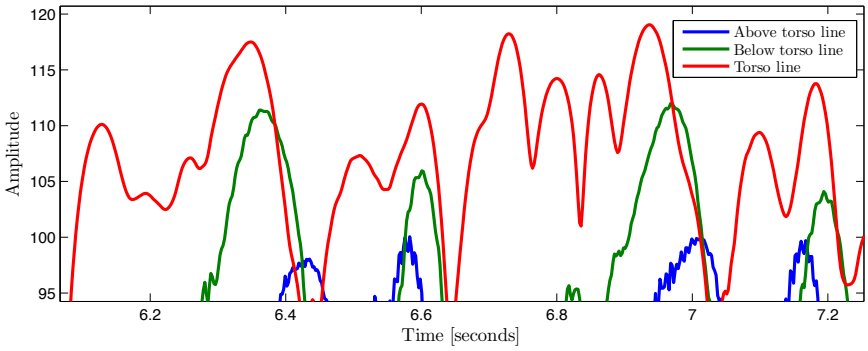

Figure 3.17: Phase differences between three Doppler slices in the spectrogram.

harmonics.

$$\beta_1 = \frac{f_2}{f_m} \qquad \beta_2 = \frac{f_3}{f_m} \tag{3.3}$$

5. **Gait amplitude ratio** (ρ): This value represents the ratio between the total micro-Doppler energy, that is spread between the fundamental gait component and gait harmonics, to the constant Doppler energy that lies close to DC in the gait-Doppler map. In the case of a human, this value can represent the ratio between the total RCS of arms and legs to the total RCS of the torso:

$$\rho = \frac{A_{f_m} + A_{f_2} + A_{f_3}}{A_{f_D}} \tag{3.4}$$

   This ratio is intended to assist in discriminating between humans and animals, since for most animals, the size of appendages compared to the main body is quite small.

6. **Phase offsets** ($\Delta\phi_1$ and $\Delta\phi_2$): These offsets are shown in Figure 3.17. This feature can potentially increase the diversity of the target recognition (with periodic motion) since it indicates how the micro-Doppler components differ in phase. These two features are only demonstrated for reference. Extraction of these features is very sophisticated. It is therefore suggested for further work.

Figure 3.18 shows an example of how to measure the values of f_m, β_1, β_2, and ρ. This plot is extracted from the gait-Doppler map by integrating the peaks in the image to a one-dimensional vector with the x-axis representing the gait-frequency and the y-axis representing the integrated amplitudes.

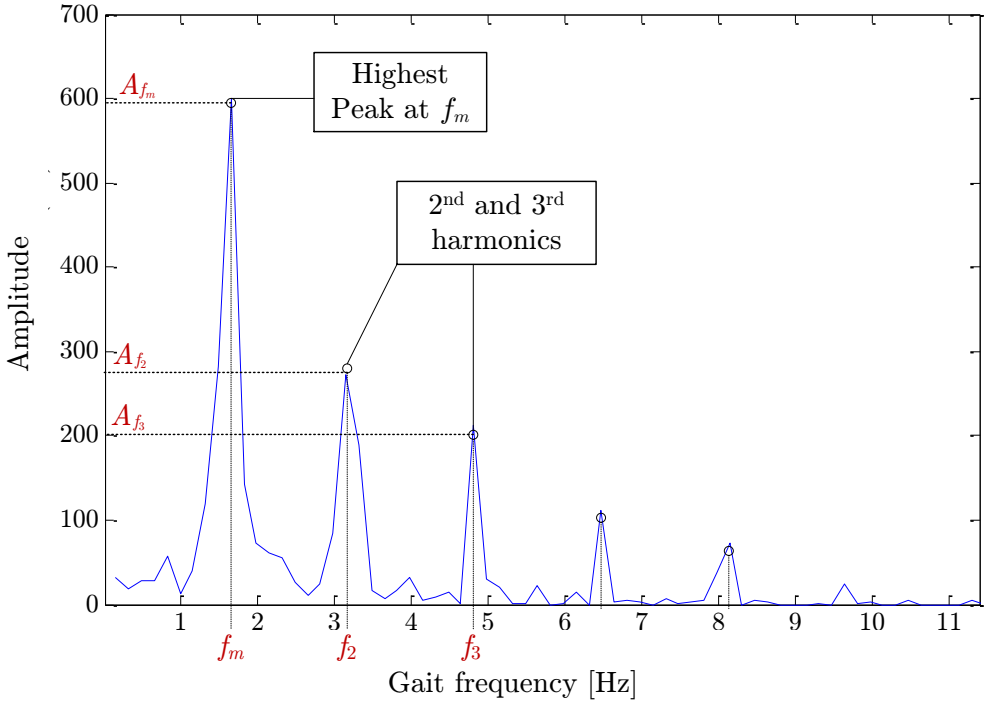

Figure 3.18: Gait fundamental component and harmonics

The integration process is done by summing up the rows of the gait-Doppler map over the target's overall Doppler bandwidth. Furthermore, the rest of the parameters are determined as follows:

- f_m is the frequency at which the highest amplitude occurs in the vector.
- f_2 and f_3 are the frequencies where the 2nd and 3rd harmonics occur, respectively.
- The total RCS of legs and arms (or the micro-Doppler components) are the total sum of the peak amplitudes at f_m, f_2 and f_3.
- The total RCS of the torso is the sum of the peak amplitudes of the torso signal intensity across the Doppler axis (the peak values at the zero gait-bin and first gait-bin).
- Phase offsets ($\Delta\phi_1$ and $\Delta\phi_2$) can be found by taking the difference in phase between two peak amplitudes along the amplitude at f_m in the gait-Doppler map.

3.7.4 The Feature Set

The following vector is generated from the feature extractor (for every burst) which forms a set of 6 features:

$$\mathbf{F} = \begin{bmatrix} v_{av} \\ B_D \\ L_s \\ \beta_1 \\ \beta_2 \\ \rho \end{bmatrix} \tag{3.5}$$

Those features will be generated for every short-time spectrogram frame. It will then pass the vector to the classifier for either training or performing classification and human detection.

3.8 Target Classification

Now that we have our feature set, we are ready to perform the target classification. The main function of the classifier is to detect the presence of a human by examining the input feature set and generating a score indicating how close the input is to a number of previous known inputs (classes). The possible outcomes that are required from the classifier output should be one of the following:

1. The target is human: when the outcome score is close to a class of human.
2. The target is not human: when the score is close to a non-human class.
3. The target is unknown: when the score is neither close to the human class nor to a non-human class.

As part of this work, two classifiers will be designed: a basic binary classifier and a multi-class artificial neural network (A-NN). Those two classifiers can work simultaneous and independently. The outcome scores of the two classifiers can be combined in the following fashion:

- The system will indicate an alarm if both classifiers detects a human
- The system will indicate an alert if one of them detects a human.

The two classifiers will require training to set the thresholds and boundaries. The training and validation of classifiers will be detailed in chapter 5.

3.8.1 Basic Classifier

The objective of this classifier is to apply early knowledge of feature dependencies features that directly relates to human motion most. As the selected features are strongly related to the dynamics of the human motion, it is possible to derive some feature dependencies from the mechanism of typical human motion. Our Experimentation shows that there is a linear relationship between the stride rate and the velocity of walking beings. That is, the higher the stride rate, the faster the movement. The other property that was suggested in literature is the possibility of distinguishing between human and other walking beings by comparing the Doppler energy that is generated by the torso to the micro-Doppler energy that is generated by the hands and legs. These two measures will be examined in chapter 5.

3.8.2 A-NN Classifier

Given the diversity and dynamics of the feature set, a classifier that can handle all or some of the possible inputs is required. The artificial neural network-based classifier is a good candidate, based on the following considerations:

- Once trained, it performs reasonably fast.
- Wide ranges of transfer functions: step, gradient, or Gaussian.
- Systematic approach to design.
- Proven to give results of high accuracy in this type of application.
- Suitable for multi-class problems.

ANN design follows the following general steps:

1. Collection of data.
2. Creating the network.
3. Configuring the network.
4. Initialising the weights.
5. Training the network.
6. Validating the network.
7. Operating the network.

Those steps will be applied and explained in chapter 5.

On the ANN design is, note that there is no systematic way for choosing the number of hidden layers and the number of neurons in each layer. Increase-until-overfit will be done to come up with the best choice, which should also give the best results. It is also a common practice not to go beyond three layers [9]. This network will give one of the two outputs we mentioned above: human or no-human. But this work intends to examine the potential of the classifier to distinguish different human activities such as running, walking, etc. Obviously, any of those results can be considered to be human, which gives the desired outcome.

Chapter 4

System Implementation

4.1 Introduction

In this chapter, we show how the final system is implemented. Full implementation was done in Matlab and was tested with a PC workstation that is capable of handling large data and processing. The interface with the system was already provided and is not part of this work. The main goal of the system is to classify human targets as they're being tracked. The Matlab code that will achieve this goal is a direct implementation of the concept design that was discussed in the previous chapter.

4.2 System Architecture

Figure 4.1 shows the overall code architecture. The blocks in the middle show the main processes of the system. The system parameters needed for each process are shown on the left. The right side shows the main figures that are used for graphical demonstration of the output of each process. The Matlab code is written in the same order. Each process is implemented as a separate Matlab function with inputs and outputs. The system parameters are defined first.

The following sections explain each process showing the implementation steps of the key processes.

4.2.1 Data Player

The data player is a software tool programmed to playback the recorded radar data. This tool was provided to us and it can be used to stream data into Matlab to emulate the radar data live-streaming capability. The data

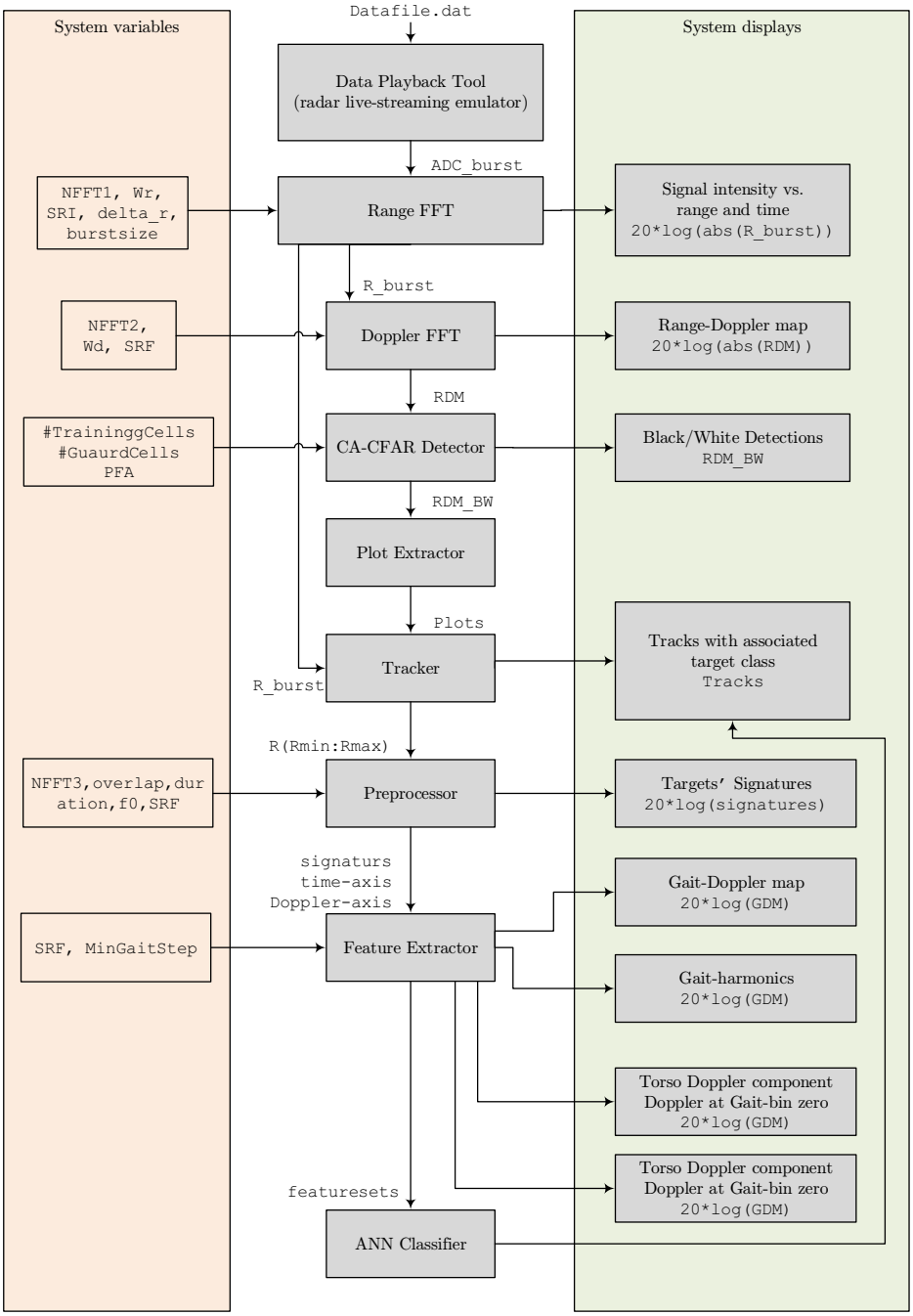

Figure 4.1: Detailed system architecture.

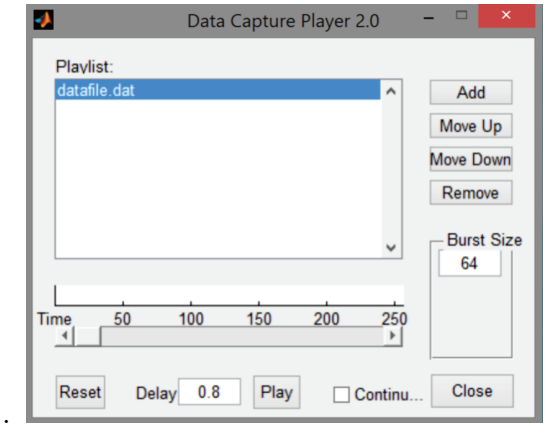

Figure 4.2: Data Playback Tool provided by RRS.

files that are recorded contain the raw samples at the output of the ADC in Figure 3.4. Each sweep is time-stamped and contains 4096 samples. We chose to playback the data in one burst at a time. The burst size is selected to be 64 sweeps. The bigger the burst size, the longer the integration time for the Doppler-FFT which will increase the SNR. Figure 4.2 shows the data playback tool that was used. The output `ADC_burst` of the Data player is loaded into a memory that Matlab can read from.

4.2.2 Range-FFT (RFFT)

The range-FFT is carried out by taking the row-FFT of the ADC samples `ADC_burst` as demonstrated in Figure 3.5. This is simply done in Matlab as follows

```
R_burst = fft(ADC_burst*.Wr, NFFT1, 2)
```

where `Wr` is a Hanning weighting window and `NFFT1` is the desired number of output FFT bins which is 4096. The output of the RFFT is a 2-sided spectrum. Since it is symmetrical only 1-side is needed, therefore we only need to consider the first `NFFT1/2` bins which is 2048. To obtain the range-axis from the frequency bins, we simply multiply each bin index by the range resolution.

The RFFT (or the range) information of the targets can be visualized via an image plot similar to those shown in Figure 3.7. To obtain the time-axis, we multiply the sweep index by SRI (provided that the first burst started at $t = 0$). The time-axis is then updated for every burst to start from the ending time of the previous burst.

4.2.3 Doppler FFT (DFFT)

The Doppler-FFT is carried out by taking the column-FFT of the RFFT matrix `R_burst` as demonstrated in Figure 3.5. This is simply done in Matlab as follows

```
RDM = fft(R_burst*.Wd, NFFT2, 1)
```

where `Wd` is also a Hanning weighting window and `NFFT2` is the desired number of bins in the output FFT. Now the time-axis in `R_burst` becomes the Doppler-axis in `RDM`. The value of `NFFT2` is dependant on the burst size (`burstsize`). The higher the burst size, the higher the `NFFT2` which gives a higher Doppler resolution. Here, we make `NFFT2`=`burstsize`.

The range-Doppler matrix can be visualized via an image plot of `RDM` (range-Doppler map). In the Doppler domain, it is necessary to have a 2-sided spectrum to separate the +ve Doppler from the −ve Doppler. To achieve this separation, it is necessary to shift the zero-frequency component of `RDM` to the center of the Doppler spectrum. This can be done in Matlab by using the function `fftshift`. The Doppler-axis is obtained by generating a linearly spaced vector of `NFFT2` elements starting from −`SRF/2` to `SRF/2`. An example of a range-Doppler map is shown in Figure 3.8. Stationary clutter resides at zero Doppler, therefore it is disregarded from the following detection process.

4.2.4 CA-CFAR Detector

The CA-CFAR detector is a direct implementation of the algorithm demonstrated in Figure 2.8. Our implementation is adapted from [11] to build the CFAR detector in Figure 2.8 for every Doppler-bin. The input to the detector is the magnitude of `RDM`. The output is a matrix of the same size with '1' and '0' corresponding to `RDM` values above or below the threshold, respectively. This can be visualized via an image plot known as the detection map or black/white image. An example of the output of the CA-CFAR detector is shown in Figure 3.9.

4.2.5 Plot Extractor

The goal of the plot extractor is to represent the target blocks in the detection map with a single plot that represents the reflection from target. This process was demonstrated in Figure 2.9. The output of the plot extractor is a set of plots. Each plot contains the time stamp, range and velocity, and an indication of the Doppler bandwidth of the target.

Plot extraction can be implemented in Matlab using the functions `bwconncomp` and `regionprops` provided in the image processing toolbox [12]. New plots are extracted for every burst.

4.2.6 Tracker

A one-dimensional tracker is implemented following the steps in section 3.5.3. The following steps summarises the tracking algorithm:

```
begin for every burst
if existing tracks count = 0
    generate a new track from each plot
if existing tracks count > 0
    for i = 1:number of plots
        for k = 1: number of tracks
            if plot(i) falls in track(i) window:
                (1) associate plot(i) to track(k)
                (2) update track(k) information
            if plot(i) doesn't fall in track(i) window:
                (1) create new track from plot
                (2) kill track(i)
         end loop k
    end loop i
end
```

Each track contains the following information:

`track id`	A unique ID number given to the track.
`track status`	`'1'` for an active track or `'0'` for dead track.
`track state`	Current range and velocity of the track.
`tracking window`	Size of the tracking window in range (`Rmin` & `Rmax`).
`track direction`	`'1'` for inbound or `'0'` for outbound.
`plot history`	The plot trail as the bursts continue to flow.
`Range-gate size`	The number of range bins surrounding the center range.
`RFFT data`	The RFFT data associated with the track.
`track signature`	Assigned once the signature is extracted.
`track features`	Assigned once the features are extracted.
`track class`	Assigned once the track is classified.

4.2.7 Preprocessor

For every existing track, this process extracts the target's micro-Doppler signature from the RFFT data as demonstrated in Figure 3.12. The Matlab

function `spectrogram` is used to carry out the signature of the targets as follows:

```
[S,f,t] = spectrogram(R_burst(rangebin,t0:t0+duration),...
                      chebwin(NFFT3,50),...
                      overlap,NFFT3,SRF);
```

where,

`S`	The output spectrogram.
`f`	The output frequency axis (Doppler axis in this case).
`t`	The time axis of the spectrogram.
`t0`	The starting time of `R_burst`.
`t0+duration`	The ending time of R_burst.
`chebwin`	A function that creates a Chebyshev weighting window.
`NFFT3`	The desired number of Doppler bins in the spectrogram.
`overlap`	The overlap between the STFT segments in the spectrogram.
`SRF`	Sweep repetition Interval.

The spectrogram is computed for every range bin contained in the track, at the desired duration of time. Then the absolute values of `S` for every range bin are added together to form the target signature as we demonstrated in Figure 3.12. Similar to the range-Doppler matrix, it is necessary to shift the zero-frequency component to the center of the Doppler spectrum to separate +ve Doppler from −ve Doppler. The overall signature can be visualized with an intensity plot such as the one in Figure 3.14. Note that the output time-axis `t` and the Doppler-axis `f` will be used in the feature extraction to determine specific features of the signature.

4.2.8 Feature Extractor

All the feature extraction processes are based on the Gait-Doppler map ,such as the one shown in Figure 3.15), the time-axis `t`, and the frequency-axis `f`. To produce the gait-Doppler map, we take the absolute value of the row-FFT of the target signature `S`:

```
GDM = abs(fft(S,[],2))
```

The time-axis in the spectrogram becomes the gait-frequency axis in `GDM` and the Doppler axis remains the same.

The next step in the feature extraction process is to extract two vectors from the `GDM`: The Doppler content at zero-gait frequency `gdm0` and the gait-harmonics vector `ghv`. An example of the first vector is shown in Figure 3.16.

An example of the second vector is shown in Figure 3.18. To extract `gdm0`, we simply take the first column of `GDM` (or `gdm(0)=GDM(:,1)` in Matlab). To extract the gait-harmonics vector `ghv`, we take each column of `GDM` and sum all the rows. This will produce the one-dimensional vector `ghv`. The sum is computed after applying a threshold to the `GDM` to illuminate the noise. Also in `ghv`, the first bin of GDM (which is the zero-gait bin) is illuminated.

The features that we intend to extract from the above are:

`v_av`	Average radial velocity of the target.
`BD`	Micro-Doppler bandwidth.
`Ls`	Stride length.
`beta1,beta2`	Gait harmonics frequency ratios.
`rho`	Gait amplitudes ratio.

To get the value of `v_av` we must get the average Doppler frequency `fd` of the target then substitute `fd` in the equation `v_av=2*c*fd/f0`, where `c` is the speed of light and `f0` is the transmit frequency of the radar which is 10 Ghz in our case. To get the value of `fd`, we find the index at which the maximum value in the vector `gdm0` occurs. This can simply be done in Matlab by using the `max` function. Once we find the index, we find the Doppler frequency value at that index. This can be determined as `fd=f(index)`.

To get the value of `BD`, we find the Doppler frequency values at which the rising edge `fu` and the falling edge `fl` of `gdm0` occurs. Then `BD=fl-fu`.

To get the value of `Ls`, we must find the fundamental gait frequency `fm` and substitute it in `Ls=v_av/fm`. The value of `fm` is found by locating the gait-frequency at which the highest value of `ghv` occurs. This is done by either using `max` function or `findpeaks` function in Matlab.

Similarly, to get the values of `beta1` and `beta2`, we must find the gait frequencies `f2` and `f3` at which the 2^{nd} and 3^{rd} harmonics occur. This can be done in Matlab by using the `findpeaks` function.

Finally, to get the value of `rho`, we must find the signal amplitudes `Afd,Afm,Af2, and Af3` at `fd`,`fm`,`f2`, and `f3`, respectively. Then these amplitudes are substituted in the equation 3.4.

4.2.9 ANN Classifier

Matlab offers a set of functions that can be used to implement and test wide varieties and types of ANN networks based on [9]. The multi-layer, feed-forward network that was previously discussed in chapter 2 is implemented for the classification process. Here we discuss the Matlab functions that's been used to build the network. The detailed training, validation and testing of the network is given in the next chapter.

To build and test the network, a large set of data is required. For every target scenario that has been recorded, we extract a set of features that represent that scenario. A target (or an output) class is defined for each scenario (or input class). The input data is normally divided into three sets: training data, validation data, and test data. Training data are presented to the network during training, and the network weights are adjusted according to its error. Validation data are used to measure the generalisation of the network and to stop training when generalisation stops improving. Testing data are used to measure the performance of the network and it has no effect on the network training. An example of creating and training an ANN network in Matlab is shown below.

```
load input_dataset
load target_dataset
net = feedforwardnet(20);
net = train(net,input_dataset,target_dataset);
```

When executing the code above, the training window will appear as shown in Figure 4.3. The function `feedforwardnet` creates the network. The number of neurons in the hidden layer is chosen to be 20. This number is found to give the highest performance in our results. The window shows that the data was divided randomly using `dividerand` function and the backpropagation method used is Levenberg-Marquardt algorithm.

Once the network is created and trained, we can use it for classification. The input to the network is a feature set representing the target. Each node at the output will produce a score value. The target is classified upon the node that produces the highest value.

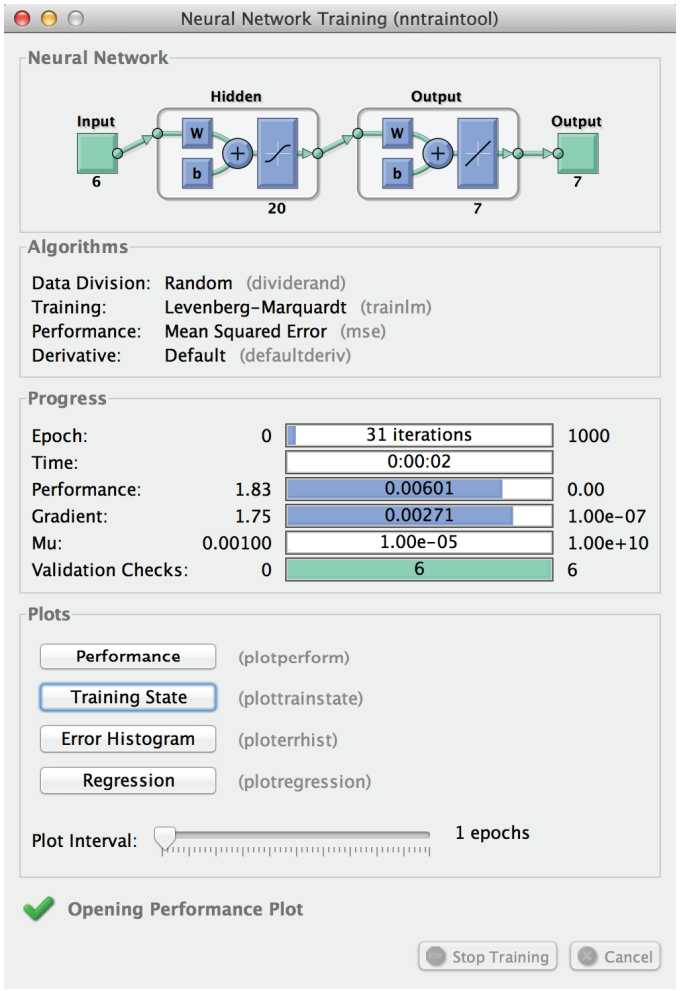

Figure 4.3: ANN training window showing the training progress.

Chapter 5

Test and Evaluation

5.1 Introduction

A full evaluation and demonstration of the human classification system are given in this chapter. The outputs of each system component are generated with relevant performance observations.

The chapter begins with an overview of the data that was collected for training and testing, as well as an overview of the type of radar that was used. The following section demonstrates the detection and tracking components. Next, a detailed demonstration of the human classification process is shown, from signature generation, feature extraction, and finally classification.

5.2 Data Collection

For the purpose of this work, radar data of real targets was captured. Those targets represent one or two human subjects moving in different directions simultaneously and performing different activities. The system will be evaluated against the data to classify humans, but also to measure the ability to discriminate between different human activities such as walking and running. If the system shows good discrimination capability, then it will most likely be able to discriminate between different types of targets such as animals and cars.

The data was captured using the RSR940 radar developed by Reutech Radar Systems. The RSR940 is a low-power, mobile, FMCW-based radar that is mainly used for border and coastal surveillance applications. This radar operates in the X-band with frequencies ranging from 9 to 10.5 GHz. It is also capable of capturing raw data and streaming it to a MS Windows-based computer via Ethernet.

With the aid of a team from Reutech, the radar was deployed to capture data of human subjects performing different activities. Sufficient data was captured to test both the tracker and the classifier, as well as to demonstrate the micro-Doppler phenomenon by pointing out the various spectral components that vary according to the different target dynamics. Each activity was captured in a period of 30 seconds with the target either inbound or outbound, and one or two subjects present at the same time. The activities are: walking with hands in pockets, marching, running, walking with a weapon, speed-walking, and walking with hands swaying.

5.3 Detector and Tracker

The objective of this test is to demonstrate and evaluate the capability of the tracker to do the following:

1. Detect the presence of moving targets using range-Doppler mapping.
2. Isolate and lock each target with a range gate.
3. Track the targets as long as they present in the beam.

The tracker will be tested against all data but only two examples are given here. Figure 5.1 shows the detection and tracking of two cases. The targets are classified as they're being tracked.

5.4 Classifier

In this context, the classifier comprises the major components involved in the classification process, namely:

1. The signature generation by means of the STFT.
2. The feature extraction process.
3. The neural network classification process.

5.4.1 Micro-Doppler Signature Extraction

The micro-Doppler signatures of six different human activities are depicted in Figure 5.2. Those are only samples of the data that were captured, and each sample is a 3-second frame of the target signature. Those signatures are generated from tracks that were manually isolated. A STFT-based method

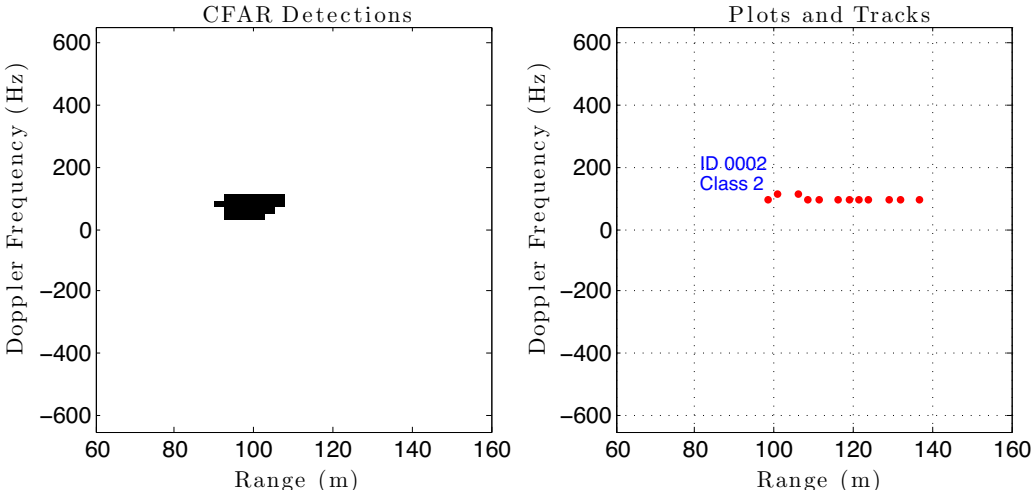

(a) walking with hands in pockets

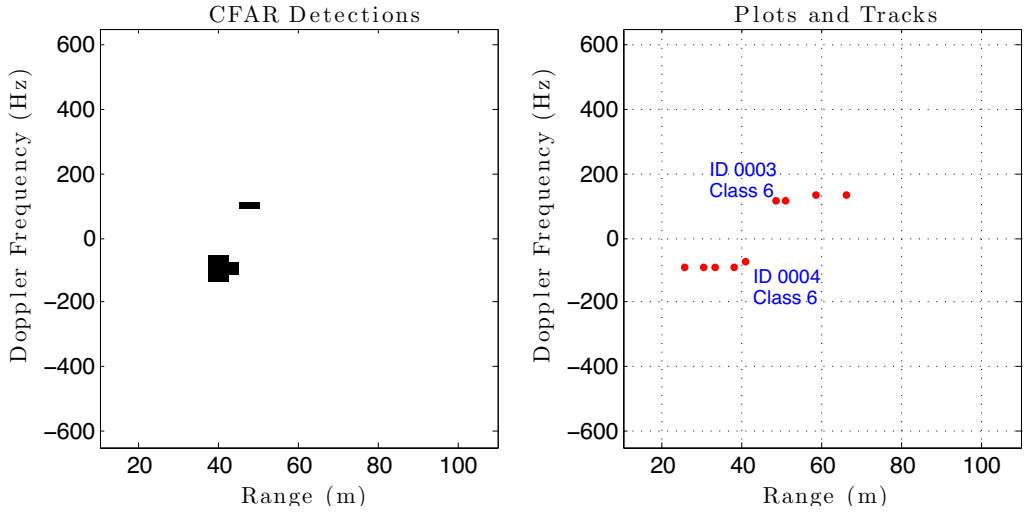

(b) Two people speed-walking

Figure 5.1: Successful detection, tracking, and classification of two cases: (a) one man walking with hands in pockets. (b) two men speed-walking.

is used to generate those signatures with $N = 128$ FFT points, 120 points overlap, and a 50-point Chebyshev window. These STFT parameters were found to give the best resolution for target signatures. For each sample, the x-axis represents time, the y-axis represents Doppler frequency shift, and the colour ranges from blue as the lowest signal intensity and red as the highest. The higher the Doppler shift, the higher the target velocity (in both directions). The limits of the Doppler frequency axis ranges from $-\text{PRF}/2$ to $+\text{PRF}/2$, where PRF is the pulse-repetition frequency. The PRF was set to 3 kHz and transmission frequency f_0 to 10 GHz.

As expected, the signatures in Figure 5.2 show unique micro-Doppler features that can be associated with the relevant target dynamics. The absence of the arms, components can be observed in Figure 5.2a and 5.2d noted in the absence of the arms micro-Doppler envelope, which also gives a higher intensity in the torso-line caused by fixing the arms to the body. A high micro-Doppler bandwidth, as well as an increased number of cycles within the same time-frame, can be observed in 5.2c resulting from an outbound running activity and in 5.2e and 5.2f resulting from the fast oscillation of legs and arms respectively. On the other hand, a lower micro-Doppler bandwidth can be observed in 5.2b resulting from the slow oscillation of marching activity. Given this ability to finely distinguish between signatures, the STFT based method, along with the specific radar parameters set for this application, gives a sufficient resolution in both frequency and time that to enable feature extraction. Finally, a straight line can be observed in all six cases showing at fixed rate. This line is a result of a discontinuity in calculating the STFT caused by the target transition from one range-bin to another. Since the feature extraction method is a transformation from the signature domain to another spectral domain, the effect of the target crossing range-bins is insignificant.

5.4.2 Feature Extraction

As discussed in chapter 3.3, feature extraction begins by taking the row-FFT of one signature frame at a time. The resulting image is called the gait-Doppler map which localises the micro-Doppler energy at different gaits. From the gait-Doppler map, two curves are extracted: one curve shows the signal intensity at the DC gait-bin and another curve shows the harmonic components across the entire gait-frequency axis. From the first curve, two features are extracted, average velocity and micro-Doppler bandwidth. Average velocity is determined by simply substituting the value of Doppler shift at the highest peak in equation 3.1. Micro-Doppler bandwidth is estimated by finding the range of frequencies between the rising and the falling edges of

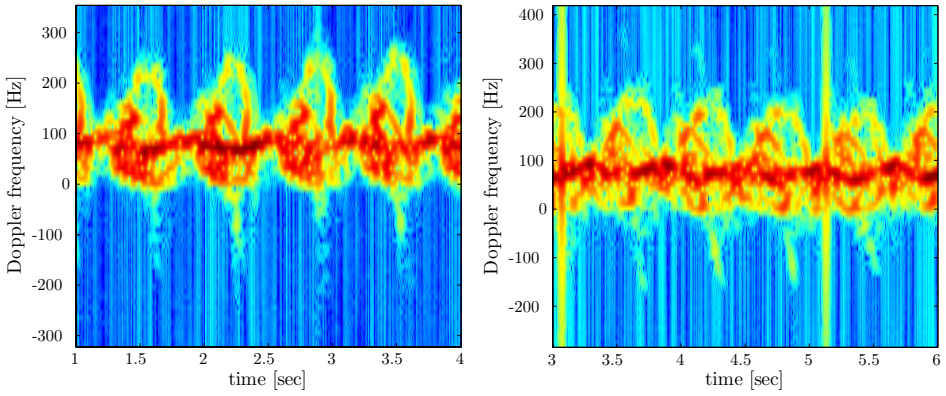

(a) walking with hands in pockets

(b) marching

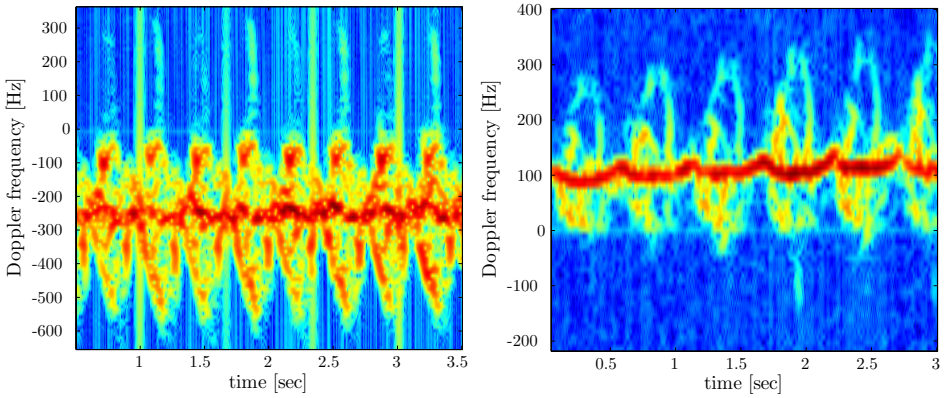

(c) running

(d) walking with a weapon

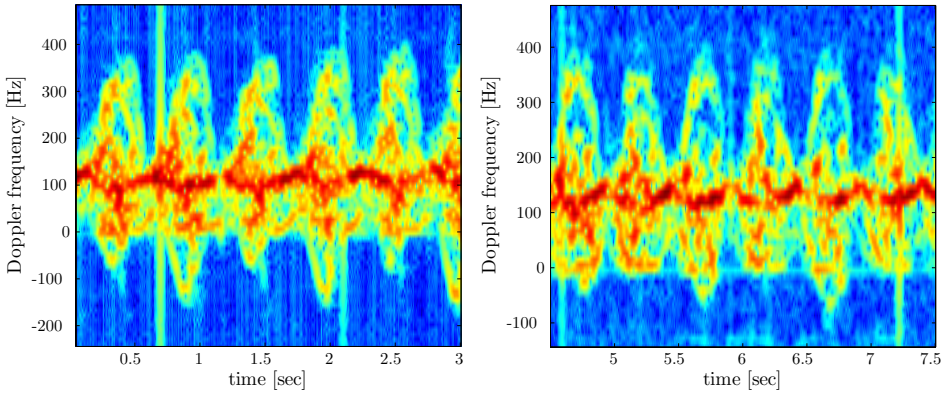

(e) speed-walking

(f) walking with arms swaying

Figure 5.2: Micro-Doppler signatures of different human activities.

Table 5.1: Sample features of different human activities.

Activity	v_{av}	L_m	$BW_{\mu D}$	$\frac{f_2}{f_m}$	$\frac{f_3}{f_m}$	RCS
(a) Walking with hands in pockets	04.86	2.93	518.00	1.80	2.80	1.23
(b) Marching	04.26	2.58	436.80	2.02	2.72	1.14
(c) Running	14.59	5.48	670.28	2.13	3.13	1.25
(d) Walking with a weapon	06.70	3.30	416.44	1.83	2.83	1.02
(e) Speed-walking	06.69	3.30	589.10	1.83	2.83	1.09
(f) Walking with hands swaying	07.91	3.95	650.00	1.99	2.99	1.06

the peak. The second curve enables the extraction of the fundamental gait-frequency which is used to find the stride-length and also to locate the second and third harmonics. From the two curves, the RCS ratio is determined.

Figures 5.3 and 5.4 demonstrate, for each sample signature in Figure 5.2, the two curves extracted from their gait-Doppler maps. The curve in Figure 5.3 is found to be a better estimator for average velocity and micro-Doppler bandwidth. The peak detector locates the highest peak, determines the frequency and records the amplitude.

The higher bandwidth can easily be observed in the activities of running, speed-walking, and walking with arms swaying. The two activities of walking with hands in pockets and marching exhibit a similar bandwidth which might cause an ambiguity in the classification process. Table 5.1 shows the extracted features from the signatures in Figure 5.2. Each row consists of the feature-vector of one activity and a single signature frame. A feature set was generated for each activity. Two scatter plots are generated in Figure 5.5 and 5.6 to show the interrelationship between human features. As observed in Figure 5.5, the data shows an almost linear relationship between stride length and velocity. The higher the human velocity, the higher the stride length. This is found to be of major importance to classify walking subjects, as one subject cannot take a long step without having to increase velocity. In Figure 5.6, the RCS ratios are scattered. It can be observed that most of the samples lie within a certain range. This is expected to assist in discriminating humans against non-human subjects, as humans have a higher RCS-ratio compared to other walking subjects such as animals. The gait-frequency ratios have no physically interpretable meaning, but can be used to ensure the right peak detection of gait harmonics. If the wrong peak is detected, the extracted features will fall outside the range typically associated with humans. Boundaries around the plots in Figure 5.5 and 5.6 can be used to define a basic classifier.

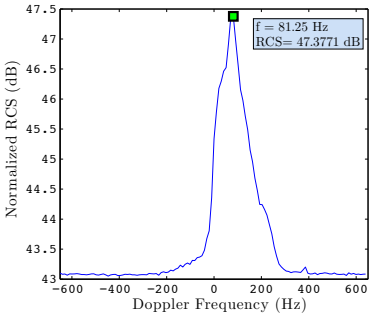

(a) walking with hands in pockets

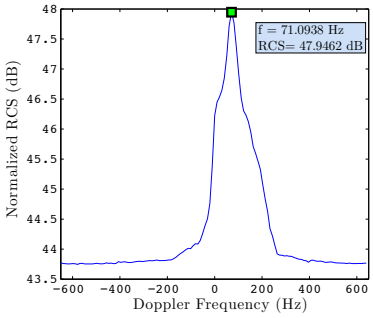

(b) marching

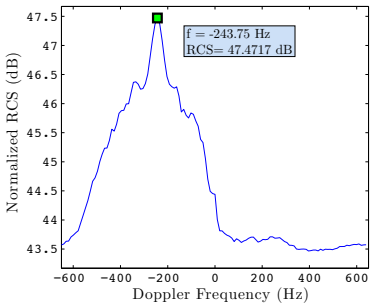

(c) running

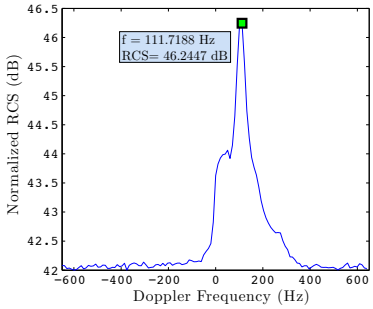

(d) walking with a weapon

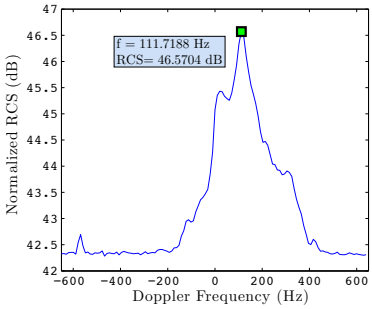

(e) speed-walking

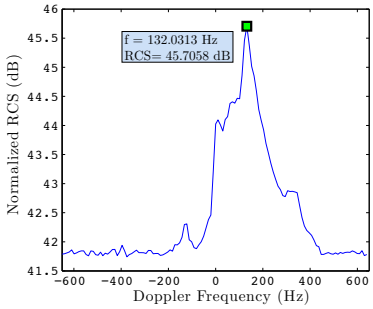

(f) walking with arms swaying

Figure 5.3: Doppler signal intensity across the DC bin of the gait-Doppler map.

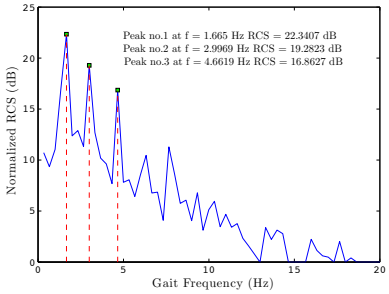

(a) walking with hands in pockets

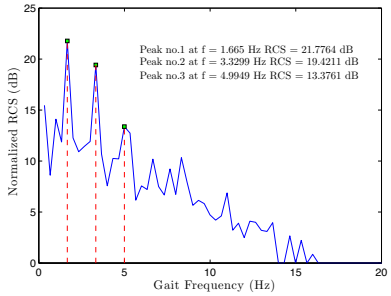

(b) marching

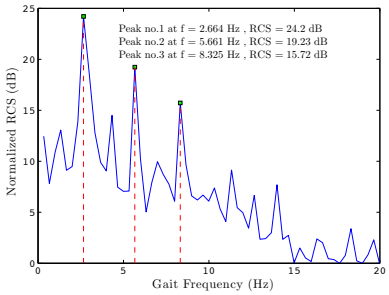

(c) running

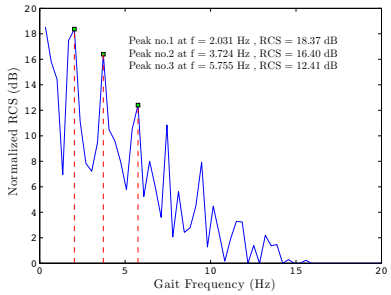

(d) walking with a weapon

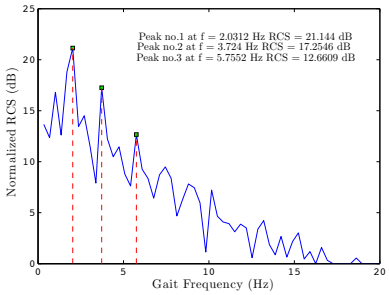

(e) speed-walking

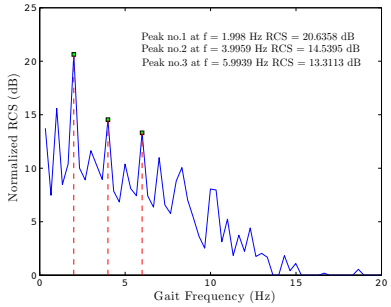

(f) walking with arms swaying

Figure 5.4: Gait fundamental component and harmonics.

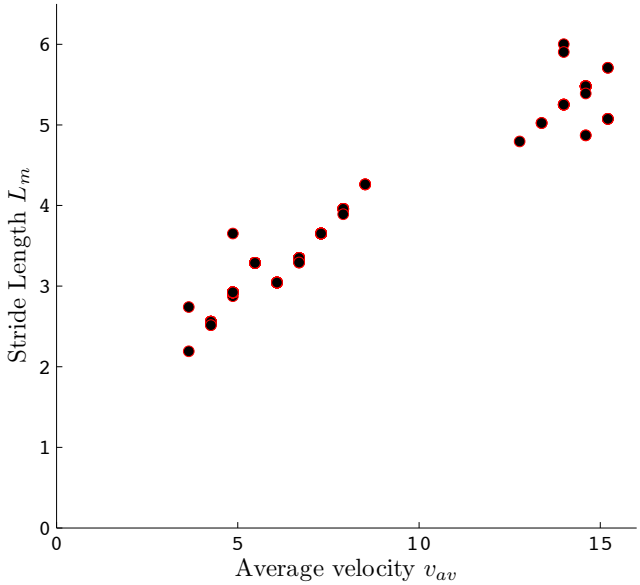

Figure 5.5: RCS ratio versus the sample number.

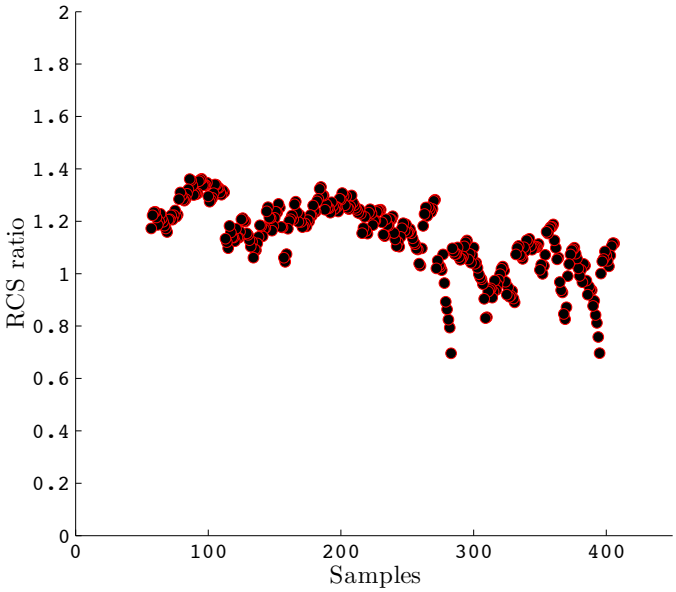

Figure 5.6: RCS ratios of the 406 samples.

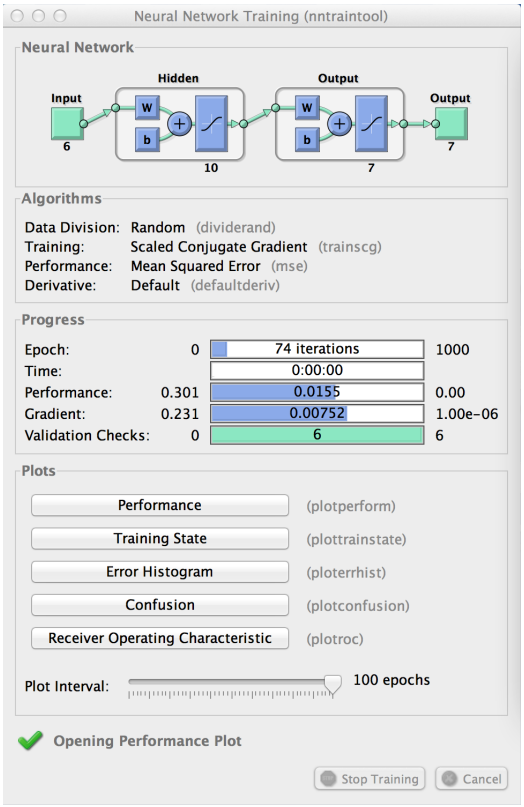

Figure 5.7: Training and validation progress.

Classification

A neural network classifier is employed for the classification process. The design procedure in section 3.8 is followed. The dataset is prepared by generating feature sets for the entire data set. From the data we have, 406 samples are generated. The samples are randomly divided in three groups: 65% are used for training, 10% for validation, and 25% are used for testing. The network is designed and trained to classify inputs against 7 classes. The different classes as well as the number of samples available for each class are listed in Table 5.2. A feed-forward multilayer network is implemented for classification with 6 neurons in the input layer, 10 neurons in the hidden layer, and 7 neurons in the output layer. These parameters are chosen such that the best classification performance is obtained. The back-propagation algorithm is used to train the network as shown in Figures 5.7 and 5.8.

The resulting confusion matrix is shown in Figure 5.9. The network output shows a high accuracy. As observed, the high number of correct classifications are shown in the green squares, and the low number of misclassified

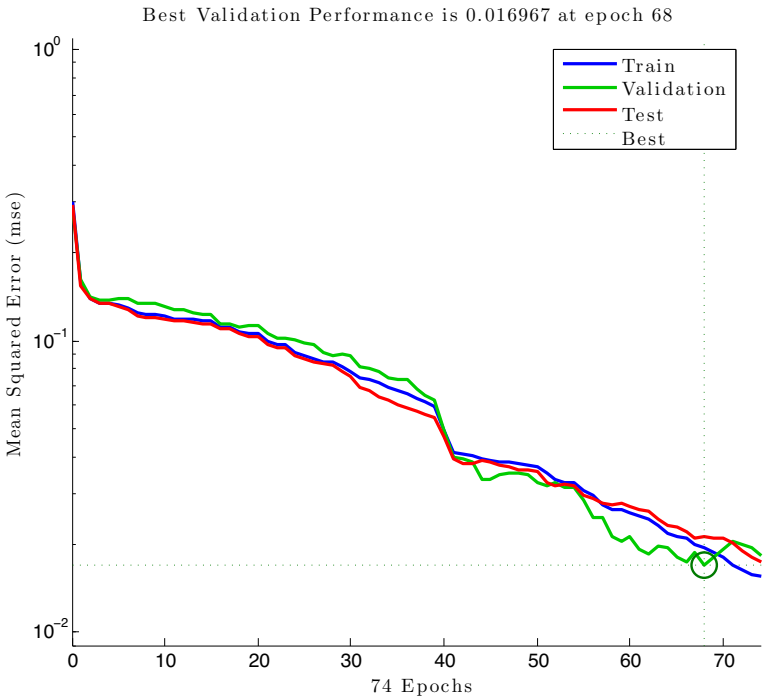

Figure 5.8: Training performance.

targets is shown in the red squares. The overall network accuracy is shown in the blue square. The marching activity was misclassified three times for walking with hands in pockets. It is believed that this error is caused by the fact that the two activities exhibit close features. Also observed is one misclassification of walking with a weapon for speed-walking. As the two activities show close values of micro-Doppler bandwidth, a slight error in the bandwidth estimation can cause this misclassification. General speaking, this classifier shows a fine distinction between activities.

Table 5.2: List of the classes.

Class	Number of samples
(1) No target (noise/clutter)	56
(2) Walking with hands in pockets	56
(3) Marching	108
(4) Running	12
(5) Walking with a weapon	39
(6) Speed-walking	71
(7) Walking with hands swaying	60
Total no. of samples	406

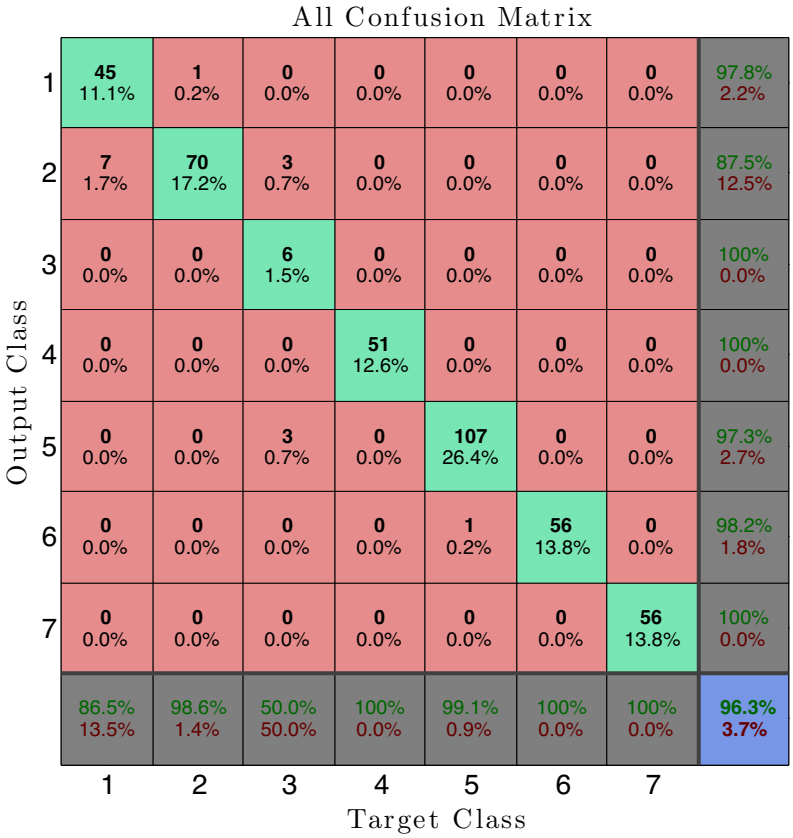

Figure 5.9: Confusion matrix showing the overall percentage of correct classification (96%).

Chapter 6

Conclusion

6.1 Discussion of Results

This work presented the design and performance analysis of a human-gait detection system based on micro-Doppler target signatures. The system comprises a first detection mechanism designed to identify and track moving targets and to assist in processing their information separately for classification. Target micro-Doppler signatures were extracted by using the STFT. A mechanism of feature extraction was developed to derive six features from signatures. A feed-forward neural network was built and trained to do the classification. The system was tested with data that was captured using an FMCW X-band radar.

Given the type of radar and the parameters that has been used, the STFT based method gave a sufficient resolution for signature extraction, and it was possible to visually distinguish between different signatures. The STFT therefore provided a good basis for feature extraction and accurate classification.

The feature extractor was developed to provide six features based on the periodicity of the target signature. Those features are average velocity, micro-Doppler bandwidth, stride length, and gait-amplitude ratios. Those features are found to represent target signatures well and assist accurate classification.

A neural network classifier was built to classify seven classes of human activities based on the six features. The classifier, combined with feature extractor, has reached an accuracy of 96%.

6.2 Contributions

This work presents a full classification system suited for practical implementation in an existing radar system. The classification method combines two methods from literature with some enhancements. High classification accuracy is achieved even though between two targets with insignificant variation in their dynamics. The feature extraction mechanism was designed in a such away to easily relate to the target dynamics.

6.3 Further Work

This work can be extended to work for more types of surface targets such as group of people, vehicles, animals, motorbikes, and birds. Also to test the system with humans that move in a high clutter area such as forests and mountains. Studying the effect of changing the aspect angle of the target's movement on the classification process can be done to to create more diverse classifier.

Advanced time-frequency analysis techniques can be used to extract a higher resolution target signature. This will improve the feature extraction process in terms of peak detection. Further enhancements in the feature extractor to extract features from a shorter signature frame can advance for classifying targets in radar scan-mode.

Bibliography

[1] V. Chen, *The Micro-Doppler Effect in Radar*. Artich House. 2010.

[2] V. Chen, H. Ling, *Time-Frequency Transforms for Radar Imaging and Signal Analysis*. Artich House. 2002.

[3] M. Richards, J. Scheer, W. Holm, *Principles of Modern Radar: Basic Principles*. SciTech Publishing. 2010.

[4] M. Richards, *Fundamentals of Radar Signal Processing*. McGraw-Hill. 2005.

[5] S. Kingsley, S. Quegan, *Understanding Radar Systems*. SciTech Publishing. 1999.

[6] P. Pace, *Detecting and Classifying Low-Probability-of-Intercept Radar*. 2nd Edition, Artich House. 2009.

[7] L. Cohen, *Time Frequency Analysis*. Prentice Hall. 1995.

[8] S. K. Mitra, *Digital Signal Processing, A Computer Based Approach*. 3rd Edition, McGraw-Hill. 2006.

[9] M. Hagan, H. Demuth, M. Beale, *Neural Network Design*. Vikas Publishing House. 2002.

[10] M. Hagan, H. Demuth, M. Beale, *Neural Network Toolbox v.7 User's Guide*. Mathworks. 2010.

[11] The MathWorks Inc. *Phased Array System Toolbox User's Guide*. Mathworks. 2011.

[12] The MathWorks Inc. *Image Processing Toolbox User's Guide*. Mathworks. 2011.

[13] The MathWorks Inc. *Signal Processing Toolbox User's Guide*. Mathworks. 2011.

[14] S. Marchand-Maillet, Y. Sharaiha, *Binary Digital Image Processing: A Discrete Approach*. Academic Press. 1999.

[15] P. Tait, *Introduction to Radar Target Recognition*. Institution of Engineering and Technology. 2005.

[16] V. G. Nebabin, *Methods and Techniques of Radar Recognition*. Artich House. 1995.

[17] F. Sadjadi, B. Javidi, *Physics of Automatic Target Recognition*. Springer Science. 2007.

[18] M. Skolnik, *Introduction to Radar Systems*. 3rd Edition, McGraw-Hill. 2001.

[19] M. Skolnik, *Radar Handbook*. 3rd Edition, McGraw-Hill. 2008.

[20] G. E. Smith, "Radar Target Micro-Doppler Signature Classification". Ph.D Thesis, University of London. 2008.

[21] J.J. Preussner, "Multiple Target Tracker and Human Classifier for Radar Application". M.Sc. Thesis, University of Florida. 2005.

[22] M. Anderson, "Design of Multiple Frequency Continuous Wave Radar Hardware and Micro-Doppler Based Detection and Classification Algorithms". Ph.D Thesis, University of Texas. 2008.

[23] M. Otero , "Application of a Continuous Wave Radar for Human Gait Recognition". *Proceedings of the SPIE on Signal Processing, Sensor Fusion, and Target Recognition*, vol. 5809, pp. 538-548. 2005.

[24] H. Sun, Z. Liu, Q. Lin, "Radar Target Recognition Based on Micro-Doppler Effect". *International Conference on Signal Processing* vol. 3, Beijing. 2006.

[25] V. Chen, "Evaluation of Bayes, ICA, PCA and SVM Methods for Classification". *NATO Science and Technology Organization, SET-080*, 2004.

[26] V. Chen, "Detection and Analysis of Human Motion by Radar". *IEEE Radar Conference*, pp. 1-4. Rome. 2008.

[27] V. Chen, "Analysis of Radar Micro-Doppler Signature With Time-Frequency Transform". *Proceedings of the Tenth IEEE Workshop on Statistical Signal and Array Processing*, pp. 463-466. Pocono Manor, PA. 2000.

[28] V. Chen, F. Li, S. S. Jo, "Micro-Doppler Effect in Radar: Phenomenon, Model, and Simulation Study". *IEEE Transactions on Aerospace and Electronic Systems*, vol. 42, Issue 1, pp. 2-21. 2006.

[29] V. Chen, "Spatial and Temporal Independent Component Analysis Of Micro-Doppler Features". *IEEE International Radar Conference*, pp. 348-353. 2005.

[30] D. Tahmoush, J. Silvious, "Radar Micro-Doppler for Long Range Front-View Gait Recognition". *IEEE 3rd International Conference on Biometrics: Theory, Applications, and Systems*, pp. 1-6. Washington DC. 2009.

[31] D. Tahmoush, J. Silvious, "Stride Rate in Radar Micro-Doppler Images". *IEEE International Conference on Systems, Man and Cybernetics*, pp. 4218-4223. San Antonio,TX. 2009 .

[32] L. Vignaud, A. Ghaleb, J. Le Kernec, "Radar High Resolution Range and Micro-Doppler Analysis Of Human Motions". *International Radar Conference - Surveillance for a Safer World*, pp. 1-6. Bordeaux. 2009.

[33] Y. Kim, H. Ling, "Human Activity Classification Based on Micro-Doppler Signatures Using a Support Vector Machine". *IEEE Transactions on Geoscience and Remote Sensing*, Vol. 47, Issue 5, pp. 1328-1337. 2009.

[34] Y. Kim, H. Ling, "Human Activity Classification Based on Micro-Doppler Signatures Using an Artificial Neural Network". *IEEE Antennas and Propagation Society International Symposium*, pp. 1-4. San Diego, CA. 2008.

[35] J. Lei, "Pattern Recognition Based on Time-Frequency Distributions of Radar Micro-Doppler Dynamics". *International Conference on Software Engineering, Artificial Intelligence, Networking and Parallel/Distributed Computing*, pp. 14-18. 2005.

[36] P. Molchanov, J. Astola, K. Egiazarian, "Ground Moving Target Classification by Using DCT Coefficients Extracted from Micro-Doppler Radar Signatures and Artificial Neuron Network". *Microwaves, Radar and Remote Sensing Symposium (MRRS)*, pp. 173-176. Kiev. 2011.

[37] C. Hornsteiner, J. Detlefsen, "Characterisation of Human Gait Using a Continuous-wave Radar at 24Ghz". *Advances in Radio Science*. Vol. 6, pp. 67-70. 2008.

[38] C. Hornsteiner, J. Detlefsen, "Extraction of Features Related to Human Gait Using a Continuous-Wave Radar". *Microwave Conference (GeMIC)*, pp. 1-3. Hamburg-Harburg, Germany. 2008.

[39] I. Bilik, J. Tabrikian, A. Cohen, "Target Classification Using Gaussian Mixture Model For Ground Surveillance Doppler Radar". *IEEE International Radar Conference*. pp 910-915. 2005.

[40] I. Bilik, J. Tabrikian, A. Cohen, "GMM-Based Target Classification for Ground Surveillance Doppler Radar". *IEEE Transactions on Aerospace and Electronic Systems*, vol. 42, Issue 1, pp 267-278. 2006.

[41] I. Bilik, J. Tabrikian, "Radar Target Classification using Doppler Signatures of Human Locomotion Models". *IEEE Transactions on Aerospace and Electronic Systems*, Vol. 43, Issue 4, pp. 1510-1522. 2007.

[42] A. Jain, J. Mao, "Artificial Neural Networks: A Tutorial". *IEEE Computer*, Vol. 29, Issue 3, pp. 31-44. 1996.

[43] J. L. Geisheimer, W. S. Marshall, E. Greneker, "A Continuous-Wave (CW) Radar for Gait Analysis". *Conference Record of the 35th Asilomar Conference on Signals, Systems and Computers*, vol. 1, pp. 834-838. Pacific Grove, CA. 2001.

[44] L. Kaiming, L. Ying, C. Long, Z. Qun, "A New Separation Method for Micro-Doppler Information of a Target with Rotating Parts". *International Conference on Communications, Circuits and Systems (ICCCAS)*, pp 1365-1369. Fujian. 2008.

[45] L. Ying, C. Long, Z. Qun, "A Novel Method for Extraction of Micro-Doppler Signal". *IEEE International Symposium on Microwave, Antenna, Propagation, and EMC Technologies For Wireless Communications*, pp. 1458-1462. Hangzhou. 2007.

[46] T. McConaghy, H. Leung, . Boss, V. Varadan, "Classification of Audio Radar Signals Using Radial Basis Function Neural Networks". *IEEE Transactions on Instrumentation and Measurement*, vol. 52, No. 6, 2003.

[47] J. Astola, K. Egiazarian, P. Molchanov, A. Totsky, "Doppler Radar Signatures Analysis by Using Joint Bispectrum-Based Time-Frequency Distributions". *International Workshop on Local and Non-Local Approximation in Image Processing (LNLA)*, pp. 137-144. Tuusula. 2009.

[48] L. Du, J. Li, P. Stoica, H. Ling, S. Ram, "Doppler Spectrogram Analysis of Human Gait via Iterative Adaptive Approach". *IEEE Electronic Letters 29th*, vol. 45, No. 3, 2009.

[49] S. Ram, Y. Li, A. Lin, H. Ling, "Doppler-Based Detection and Tracking of Humans in Indoor Environments". *Journal of The Franklin Institute - Advances in Indoor Radar Imaging*, Vol. 345, Issue 6, pp. 679-699. 2008.

[50] S. Ram, H. Ling, "Simulation of Human Microdopplers Using Computer Animation Data". *IEEE Radar Conference*, pp. 1-6. Rome. 2008.

[51] S. Ram, H. Ling, "Microdoppler Signature Simulation of Computer Animated Human and Animal Motions". *IEEE Antennas and Propagation Society International Symposium*, pp. 1-4. San Diego, CA. 2008.

[52] S. Ram, H. Ling, "Analysis of MicroDopplers from Human Gait Using Reassigned Joint Time-Frequency Transform". *IET Electronic Letters*. Vol. 43, Issue 23. 2007.

[53] C. Hornsteiner, J. Detlefsen, "Feature Extraction Related to Human Gait for a Continuous-Wave Radar". *Frequenz*, Vol. 62, Issue 9-10, pp 262-264. 2008.

[54] F. Gustafsson, U. Orguner, S. Bjorklund, "Human Gait Parameter Estimation Based on Micro-Doppler Signatures Using Particle Filters". *IEEE International Conference on Acoustics, Speech and Signal Processing*, pp. 5940-5943. Prague. 2011.

[55] K. Kim, I. Sik Choi, H. Kim, "Efficient Radar Target Classification Using Adaptive Joint Time-Frequency Processing and Neural Network". *IEEE Transactions on Antennas and Propagation*, vol. 48, No. 12, pp. 1789-1801. 2000.

[56] L. Yongxiang, C. Hangyong, Li Xiang, Zhuang Zhaowen, "Radar Micromotion Target Resolution". *International Conference on Radar*, pp. 1-4. Shanghai. 2006.

[57] M. Anderson, R. Rogers, "Micro-Doppler Analysis of Multiple Frequency Continuous-Wave Radar Signatures". *Radar Sensor Technology Proceedings of SPIE*, vol. 6547, 2007.

[58] Z. Zhang, P. Pouliquen, A. Waxmant, A. G. Andreou, "Acoustic Micro-Doppler Gait Signatures of Humans and Animals". *41st Annual Conference on Information Sciences and Systems*, pp. 627-630. Baltimore, MD. 2007.

[59] Y. Li, L. Du, H. Liu, "Moving Vehicle Classification Based on Micro-Doppler Signature". *IEEE International Conference on Signal Processing, Communications and Computing (ICSPCC)*, pp. 1-4. Xi'an. 2011.

[60] P. Setlur, M. Amin, F. Ahmad, "Urban Target Classifications Using Time-Frequency Micro-Doppler Signatures". *9th International Symposium on Signal Processing and Its Applications*, pp. 1-4. Sharjah. 2007.

[61] G. E. Smith, K. Woodbridge, C. J. Baker, "Micro-Doppler Signature Classification". *International Conference on Radar*, pp. 1-4. Shanghai, 2006.

[62] G. E. Smith, K. Woodbridge, C. J. Baker, "Template Based Micro-Doppler Signature Classification". *European Radar Conference* , pp. 158-161. Manchester, 2006.

[63] D. Tahmoush, J. Silvious, "Radar Stride Rate Extraction". *13th International Machine Vision and Image Processing Conference*, pp. 128-133. Dublin. 2009.

[64] A. Alejos, M. Sanchez, D. Iglesias, I. Cuifias, "Real-time Method for Human Presence Detection by Using Micro-Doppler Signatures Information at 24GHz". *IEEE Antennas and Propagation Society International Symposium*, pp. 1-4. Charleston, SC. 2009.

[65] S. Marple, "Sharpening and Bandwidth Extrapolation Techniques for Radar Micro-Doppler Feature Extraction". *Proceedings of the International Radar Conference*, pp. 166-170. 2003.

[66] T. Thayaparan, L. Stankovic, I. Djurovic, "Micro-Doppler-Based Target Detection and Feature Extraction in Indoor and Outdoor Environments". *Journal of The Franklin Institute - Advances in Indoor Radar Imaging*, vol. 345, Issue 6, pp. 700-722. 2008.

[67] Z. Qun, G. Hual,G. Ying, B. YouqingI, "Separation of Micro-Doppler Signal Using an Extended Hough Transform". *International Conference on Communications, Circuits and Systems Proceedings*, vol.1, pp. 361-365. Guilin. 2006.

[68] S. Gurbuz, W. Melvin, D. Williams, "Detection and Identification of Human Targets in Radar Data". *Proceedings of the SPIE - Signal Processing, Sensor Fusion, and Target Recognition XVI*, vol. 6567. 2007.

[69] D. Tahmoush, J. Silvious, "Time-Integrated Range-Doppler Maps for Visualizing and Classifying Radar Data". *IEEE Radar Conference (RADAR)*, pp 372-374. Kansas City. 2011.

[70] T. Thayaparan, S. Abrol , E. Riseborough, Stankovic, Lamothe and Duff, "Analysis of Radar Micro-Doppler Signatures From Experimental Helicopter and Human Data". *IET Radar, Sonar, and Navigation*, vol. 1, Issue 4, 2007.

[71] A. Stove, "A Doppler-Based Target Classifier Using Linear Discriminants and Principal Components". *IET Seminar on High Resolution Imaging and Target Classification*, pp 107-125. London. 2004.